공학박사학위논문

Application of Solid-State Nanopore for Protein-Protein Interaction Inhibitor Screening

2019년 8월

서울대학교 대학원

재료공학부

채 홍 식

Application of Solid-State Nanopore for Protein-Protein Interaction Inhibitor Screening

A DISSERTATION SUBMITTED TO
DEPARTMENT OF MATERIALS SCIENCE AND ENGINEERING
SEOUL NATIONAL UNIVERSITY

FOR THE DEGREE OF
DOCTOR OF PHILOSOPHY

HONGSIK CHAE
August 2019

Abstract

Owing to the sub-single-molecule resolution with ultra-fast, and high-throughput electrical reading characteristics, solid-state nanopores have attracted researchers for analyzing biophysical properties of biomolecules. Past decade, researches on solid-state nanopores have focused on the features of nucleic acids such as transport phenomena, and especially, sequencing of deoxyribonucleic acid (DNA) molecules. Recently, proteins are rapidly becoming the prime target for the solid-state nanopore research. In this dissertation, the recent achievements of protein molecule detection are discussed, which include: i) protein-protein interactions (PPIs) and its inhibition by small-molecule drug, ii) conformational change induced by inhibition of PPIs, and iii) development of drug screening platform using low-noise solid-state nanopores.

Firstly, we monitored the interaction between the p53 transactivation domain (p53TAD) and mouse double minute 2 (MDM2) as well as its inhibition by Nutlin-3 using solid-state nanopores. The positively charged MDM2 (isoelectric point; pI = 9.0) is driven through a nanopore by the applied negative potential. However, the net charge is altered to negative as a result of the interaction with negatively charged p53TAD (pI = 3.6), resulting that the capture frequency of MDM2 is significantly reduced at the negative electric potential. In this stage, the addition of Nutlin-3 into the p53TAD/MDM2 mixture inhibits the interaction of p53TAD/MDM2, thereby liberates MDM2 from the complex. We observed the restored event frequency of MDM2 in this case, reflecting the inhibition of the interaction between p53TAD and MDM2. However, this approach is only applicable to the protein system, where the change in net charge is employed.

Advanced from the monitoring event frequency, we attempted to monitor the drug-induced conformational changes of p53TAD-MDM2 fusion protein using solid-state nanopores. To effectively detect conformational changes resulting from the protein-protein interaction, we designed a fusion protein MLP (MDM2-linker-p53TAD), where p53TAD and MDM2 are connected by a 16 amino acid residue long linker. The globular conformation of MLP exhibited a single-peak translocation event (type I), whereas the dumbbell-like conformation of Nutlin-3-bound MLP showed a double-peak signal (type II). The proportion of double-peak to single-peak signals increased from 9.3 % to 23.0 % as Nutlin-3 concentration increased from 1-fold to 10-fold molar ratio to the MLP concentration. The translocation kinetics of the two different MLP conformations with varied applied voltage were analyzed. Further, the fractional current of the intra-peak of the double-peak signal was analyzed, probing the structure of our designed protein complex.

In the last part, we demonstrate solid-state nanopore titration of three different small-molecule drugs (Nutlin-3, NSC, and SC) into MLP to quantitatively evaluate the binding affinity of drug molecules. In order to reveal the resolution for discriminating double-peak signal in the measurement system, we introduced a modified MLP protein complex (mutant MLP; mMLP) by replacing p53TAD (residues 15-29; SN15) with an amino acid residue $(GGGS)_3GGS$ to form a dumbbell shape without any drug treatment. Since SN15 is exchanged with the amino acid repeat within mMLP, there is no binding motif toward MDM2, thereby exhibits all-dumbbell-shaped conformation in solution. The maximum type II event fraction revealed as ~0.84 for all-dumbbell shaped mMLP, implying resolution limitation for the measurement system. Based on the increase in type II fraction

from conformational change of MLP induced by drug molecules, we observed different type II fraction for each drug molecule. By fitting the simple binding model to the type II fraction yields a dissociation constant (K_d) of the drug molecule, showing K_d as 594±39, 807±12, and 2650±177 nM for Nutlin-3, NSC, and SC, respectively. This approach of nanopore sensing may be extendedly employed in screening of PPI inhibitors and protein conformation studies.

Keywords: solid-state nanopores, single-molecule detections, protein-protein interactions, protein conformations, drug screenings
Student Number: 2012-23933

Table of Contents

List of Tables

Chapter 1.

Chapter 2.

Chapter 3.

List of Figures

Chapter 1.

ΔI of translocation signals. (c) Scatter plots of translocation duration versus normalized conductance drop for proteins studied using the glass capillary nanopores. Each scatter plot represents translocation events of green fluorescent protein (GFP, pink), GFP–GFP dimer (FP, orange), BSA (red), IgG (green), and RNA polymerase (RNAp, navy). All the results are summarized in the rightmost graph in the second row. (d) The nanopore detection limit on the mapping of a protein expressed as the interplay of the in-pore molecular diffusivity and the electrophoretic drift velocity. (e) Nanopore translocation time histogram of proteinase K (left) and RNase (right) at 100–200 mV, with red-shadowed regions indicating the signal loss caused by limited temporal resolution of a nanopore. The y-axis shows arbitrary units. Figure adopted from ref. 20.

Figure 1-4. Protein–protein interaction analysis. a) Analysis of the antibody–PBCV-1 virus interaction using the glass nanopore and resulting translocation signals. b) Analysis of the HIV antigen gp120, an antibody, and a protein (BSA and FBS) using the nanopore according to the current drop magnitude. c) Nanopore-based analysis of inhibition of the p53–MDM2 interaction by a drug (Nutlin-3). The cartoons on the interactions between molecules and resulting translocation signals are presented. Figure adopted from ref. 20.

Figure 1-5. Measurement of DNA translocation using complementary metal-oxide semiconductor nanopore system with high-bandwidth filtering frequencies. Unresolved peak at 1 MHz filter frequency becomes resolved at sub-micro second level at 5 MHz.

Chapter 2.

Figure 2-1. Illustration of a nanopore detection. (a) A molecular model for free and Nutlin-3-bound MLP fusion protein. GST, MDM2, and Nutlin-3 are colored in red, blue, and yellow, respectively. (b) Schematic of a nanopore detection where MLP traverses through a silicon nitride (SiN) pore with effective thickness h_{eff} = 7 nm and pore diameter d_p = 8 nm (not to scale). Left, single-spike signal expected from the globular structure (type I). Inhibition of p53TAD/MDM2 interaction by Nutlin-3 elongates the linker to transform MLP into a dumbbell-like structure. Right, expected distinctive double-peak nanopore signal from tMLP translocation (type II).

Figure 2-2. $^{15}N–^{1}H$ HSQC spectra of MLP with and without Nutlin-3. Crosspeaks of free (blue) and Nutlin-3-bound MLP (red) are shown. MLP was treated with Nutlin-3 at the molar ratio of 1:5. Green circles and arrows indicate the recovered crosspeaks after addition of Nutlin-3. Data provided

by KRIBB (Dr. Seung-Wook Chi's group)

Figure 2-3. (a) I–V characteristic of the low-noise solid-state nanopore device. A schematic structure of the device and a transmission electron micrograph of the nanopore is shown in inset. (b) Continuous current trace of nanopore signal with respect to the molar ratio of Nutlin-3 to the MLP as free (black), 1:1 (red), 1:5 (green), and 1:10 (blue). (c) Percentage of detected type I and type II signals versus Nutlin-3 concentration. Concatenated events of the proteins for free (d), 1:1 (e), 1:5 (f), and 1:10 (g). Among single-peak type I signals (black), a distinctive finger print-like double peak is shown in type II events (red). Type II events were found only in the mixture of MLP and Nutlin-3. Data were acquired at 4.16 MHz sampling rate and low-pass filtered at 500 kHz.

Figure 2-4. Scatter plot of fractional current drop versus dwell time for free (a), 1:1 (b), 1:5 (c), and 1:10 (d) molar ratios of MLP and Nutlin-3. Type II events (red star) were discriminated in type I events (black square) in the scatter plots. N ~2000 events were collected for each Nutlin-3 concentration. Dwell time histogram of type I and type II events for free (e) 1:1 (f), 1:5 (g), and 1:10 (h). Only type I events are available for (a) and

Figure 2-5. Histogram of dwell time for type II inter-event. Inset (a) represents the local dwell time of type II event (t_H, t_M and t_L). Dwell time histogram was fitted by the Gaussian function for t_H (a) and t_M (b), while dwell time histogram for t_L was fitted exponential decay function with characteristic time of 2.32, 2.44, and 2.15 μs for 1:1, 1:5, and 1:10, respectively.

Figure 2-6. Power spectrum of silicon nitride nanopore signal with 1 M KCl in 1×PBS solution under 200 mV electric potential. Data was acquired using 4.16 MHz sampling rate and low-pass filtered at 500 kHz.

Figure 2-7. Scatter plot of fractional current drop versus dwell time for free (a), 1:1 (b), 1:5 (c), and 1:10 (d) molar ratios of MLP and Nutlin-3. Type II events (red star) were discriminated in type I events (black square) in the scatter plots. N ~2000 events were collected for each Nutlin-3 concentration. Dwell time histogram of type I and type II events for free (e) 1:1 (f), 1:5 (g), and 1:10 (h). Only type I events are available for (a) and (e). Dwell time histograms were fitted using eq (2) (see text) for extracting free parameter of in-pore diffusion coefficient D_p and drift velocity v_d.

Figure 2-8. (a) Scatter plots of fractional current drop versus dwell time for type I and type II at the different voltages. (b) Dwell time distributions for type I and type II event varying electric potential. All histograms are fitted by 1D diffusion-drift model (see main text) ($R^2 > 0.95$). (c) Drift velocity of type I and type II event as a function of applied voltage. The drift velocity was extracted from the 1D diffusion-drift model and linearly increases to the increased applied voltage. (d) Normalized capture rate versus applied voltage.

Figure 2-9. Fractional current drop histogram of type II intra-event. Fractional current drop histogram of I_H (a), I_M (b), and I_L (c) of type II event. Inset (a) represents the local fractional current drop of type II event (I_H, I_L and I_M). Fractional current drop histogram of local peak parameters for 1-fold (red), 5-fold (green) and 10-fold Nutlin-3 added MLP (blue). All histograms were fitted by the Gaussian function.

Chapter 3.

Figure 3-1. Illustration of nanopore titration. (a) Nanopore detection of the globular shaped MLP (i) and the drug-bound dumbbell shaped tMLP (ii). The expected peak signal of MLP with and without drug molecule addition.

A single-peak signal of MLP molecule translocation and a characteristic double-peak signal of tMLP are schematically depicted. Nanopores with a diameter of ~8 nm were drilled by focused electron beam and the representative electron micrograph of is shown in the inset (scale bar is 10 nm). (b) A conceptual sketch of estimating K_d value of inhibitors from the type II event fraction.

Figure 3-2. Discriminating type I and type II events through nanopore signal of mMLP molecule. (a) Scatter plots of $\Delta I/I_0$ *versus* dwell time for type I and type II events low-pass filtered at the indicated frequency (N ~ 2,000 events). Distortion of a representative type II event filtered to the one identical data (inset). Green arrow represents the current fluctuation of base line upon increased cutoff frequency. (b) Type II event fraction as function of cutoff frequency. The maximum type II fraction was found at f_c = 500 kHz. (c) Normalized capture rate.

Figure 3-3. Comparison of the intra-molecular structure of tMLP and mMLP. Scatter plot of normalized current drop *versus* dwell time for MLP with 15-fold Nulin-3 (a) and mMLP translocation event (b). Type I (black square) and type II events (red star) are discriminated in the scatter plots. The representative type II signal is presented in the inset. (c-e) Histogram of

normalized current drop of the intra-peak in the type II signal of tMLP (black) and mMLP (red). I_P, I_M, and I_L represent the normalized current drop of GST-p53TAD (I_P), MDM2 (I_M), and amino acid linker (I_L) part in the tMLP and mMLP, respectively. All histograms are fitted by the Gaussian function ($R^2 > 0.92$).

Figure 3-4. Nanopore titration of potential inhibitor of the interaction between p53 and MDM2. (a) Chemical structure of inhibitors (Nutlin-3, NSC66811, and SC204072). ((4-amino-6-((4-methoxyphenyl)amino)-1,3,5-triazin-2-yl)methyl 4-methylpiperazine-1-carbodithioate (MMC) is introduced as a negative control. (b) Calibrated type II fraction *versus* molar ratio of drug to MLP along with the fits to the binding model (eq. 1) with K_d as a free parameter.

Figure 3-5. ITC measurement of p53TAD and MDM2 interaction inhibitors. The dissociation constant (K_d) was determined by titrating 50 μM of Nutlin-3 (a), 50 μM of NSC66811 (b), and 75 μM of SC204072 (c) to 5 μM of MLP sample, respectively. Data provided by KRIBB (Dr. Seung-Wook Chi's group)

Chapter 1. Introduction

1.1. Solid-state nanopore technology

Transport of biomolecule through biological pore such as α-hemolysin or *Mycobacterium smegmatis* porin A (MspA) in cell nucleus plays an important role in biological activity. In order to study the transport phenomena, a single α-hemolysin pore has been introduced in free-standing lipid bilayer membrane to construct a single channel. Small biomolecules such as nucleic acids and proteins (< ~50 kDa) could pass through the α-hemolysin by diffusional motion but also, in this system, the electric potential can be applied across the membrane that enables the charged biomolecules to be dragged toward the nanopore by electrophoretic force. Since the diameter of the biological nanopore is fixed, transport of biomolecule larger than the nanopore is physically not preferable. Therefore, there have been intensive works done in engineered the biological nanopore for modifying nanopore diameter to access larger biomolecule translocation (> 50 kDa), that lead to expand the target analytes. However, biological nanopore has still limitation for applying harsh chemical and physical experimental condition, where the analyte might undergo (i.e., pH, high ionic strength, temperature, and external pressure, etc.).

Solid-state nanopores are artificial system that mimic the structure of biological pore using inorganic solid materials, such as silicon nitride (SiN). While biological nanopore utilizes the existing protein nanopores with fixed

structure (thickness, pore diameter, etc.), the size of solid-state nanopore can be tuned as desired size and relatively stable in the harsh environments.[1]

Figure 1-1 depicts the schematic illustration of solid-state nanopore measurement principle. The free-standing SiN membrane, that contains a single nanopore penetrating the membrane, divides the system into two parts (top and bottom chamber). Then, electrolyte, such as potassium chloride (KCl), is filled in both chambers. In each chamber, Ag/AgCl electrode is introduced for applying electric potential across the membrane. Since the nanopore is the only conducting path (SiN is insulating material with dielectric constant of $\varepsilon_r \sim 7$), the potential is significantly dropped near the nanopore, developing electric field gradient. Then, the charged ions are passes toward nanopore and the steady-state ionic current is measured. Here, the addition of target biomolecule such as DNA or protein leads to the molecule dragged electrophoretically by electric field near the pore. Based on the resistive pulse technique, the partial blockage of nanopore by the biomolecule causes the current drop and the complete passage results recover to steady-state current so that nanopore system detects the spike shaped signal from a single molecule translocation. The larger volume blocked in nanopore, the larger current drop amplitude (ΔI) is obtained. Also, the longer molecule passes, the longer dwell time (t_d) can be measured. In current trace, the interval of inter-event duration represents the event frequency, which is a function of the concentration of analyte, and applied

potential, etc.

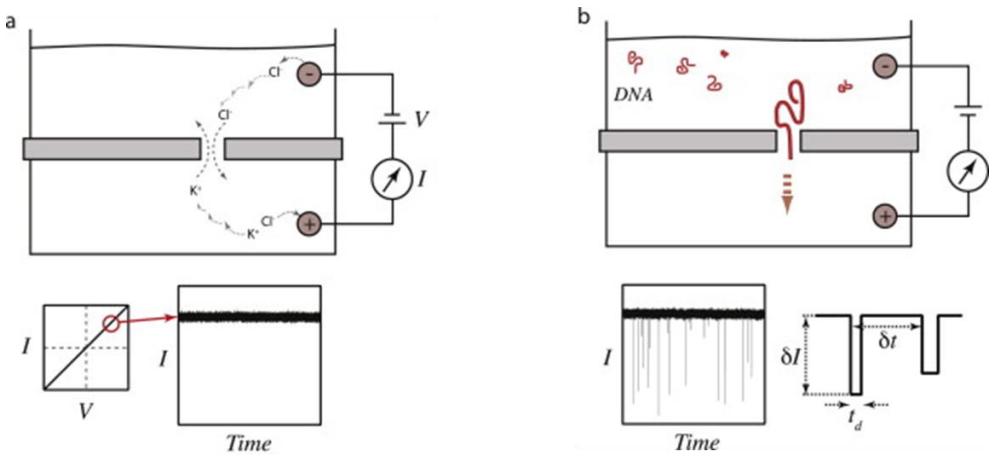

Figure 1-1. The basics of nanopore measurements. Schematic illustration of nanopore measurement principle. (a) The divided section by free-standing silicon nitride membrane is filled with potassium chloride solution. Application of electric potential induces electric field near the pore, inducing electrophoretic force to the ions. The flow of ions can be measured as steady-state current by applied potential. (b) Measurement of the pass-through signal of the charged biomolecules. The partial blockage of pore by the molecule reduces the ionic current, and recovered after complete translocation, resulting resistive pulse as a spike signal. Adopted from ref. 1.

1.1.1. Solid-state nanopore for protein sensing

Although nucleic acids have been at the center of attention over the past decade, proteins are rapidly becoming the prime target for the solid-state nanopore research.[2-9] Unlike nucleic acids, each protein has a unique 3D structure and heterogeneous charge profiles. These biophysical properties of protein yield different behaviors from those of nucleic acids, including high pH responsiveness, conformational changes, and specificity in translocation and complexation with other proteins, which are directly reflected in the nanopore signals. In accordance with the ability of the solid-state nanopore sensing to collect and analyze information on proteins, e.g., charge, size, shape, and complexation with other molecules, various properties of proteins have been studied in the nanopore field.

1.1.1.1. Historical perspective of protein detection using nanopores

In 1987, Singer *et al.* reported the first idea of the protein translocation through a biological nanopore.[10] In the early sketch of the idea, translocation of a peptide molecule with a few subdomains through a translocator protein inserted in the lipid bilayer, conceptually indicated the feasibility of detecting protein translocation by means of the biological nanopore. Nevertheless, the translocation of a single protein molecule in a nanopore emerged in the 2000s[11], owing to the difficulties in protein translocation through α-hemolysin nanopore and the fabrication of the solid-state nanopore device. In 2006, Han *et al.* first reported protein translocation through the solid-state nanopore.[4] Translocation of a single bovine serum albumin (BSA) protein molecule across a 20-nm-thick SiN membrane with a 50-nm-diameter pore was detected. The nanopore structure with relatively large pore sizes (in comparison with the devices used for DNA experiments) or with the dimensions comparable to those of the analyte proteins was widely accepted and similarly adopted in other studies on the nanopore protein detection. Figure 1-2 shows the remarkable research result in time line. Thanks to the improvement of fabrication techniques, solid-state nanopores have highlighted for its mass production, high throughput, and device stability. From single protein molecule detection, various biophysical properties of proteins have been investigated by using solid-state nanopore.

Application of protein-protein interaction was firstly demonstrated by Uram *et al.* in 2006[12]. In 2011, research on folding/unfolding state of protein was reported by Freedman *et al.*[13] In 2012, protein-drug interaction was demonstrated by Tavassoly *et al.*, monitored by current drop distribution in protein nanopores.[14] At the same year, Yusko *et al.* reported the translocation signal of time-dependent fibrilization of Aβ.[15] In 2013, Plesa *et al.* discovered data distortion by fast translocation of protein molecule, and requirement of the high-bandwidth measurement has emerged.[16] In 2014, Larkin *et al.* demonstrated the high-bandwidth detection of sub-50 kDa protein molecule.[17] In 2016, Kennedy *et al.* attempted to resolve sequence of amino acid residue of protein using sub nanometer pores.[18] By the same year, Kwak *et al.* demonstrated the protein-protein interaction and its inhibition of small-molecule by using low-noise solid-state nanopores.[19]

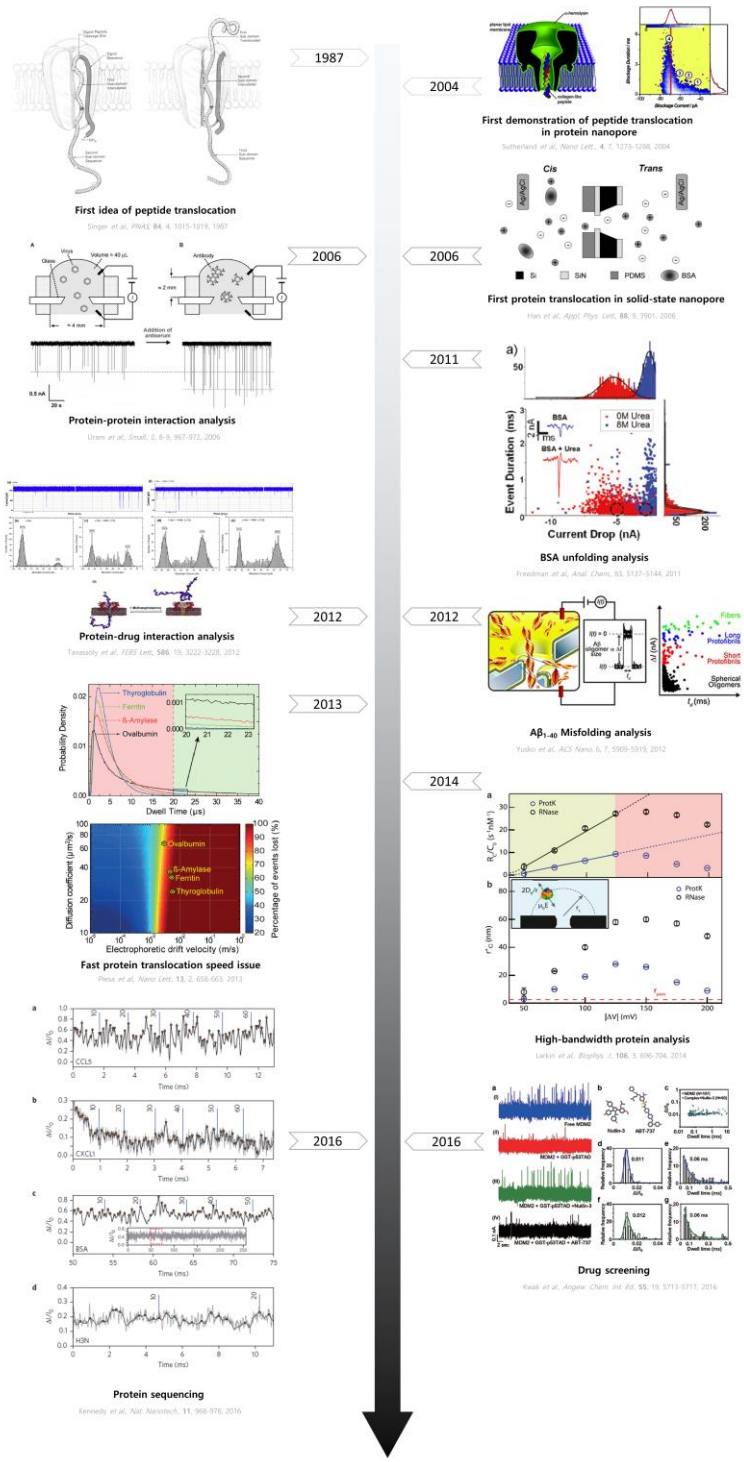

Figure 1-2. Time line of key nanopore result of biophysical property of proteins. Figures are adapted from ref. 4, 10-19.

1.1.1.2. Biophysical properties in protein translocation[20, ①]

1.1.1.2.1. Net charge of proteins

A property of a protein that determines its translocation through the nanopore is the net charge; protein molecules generally have relatively low charge density in total as compared to DNA. Therefore, the net charge of proteins can be easily modified or even the sign of the charge can be switched by a slight change in the electrolyte pH. On the basis of this phenomenon, Firnkes *et al.* investigated the changes in the translocation mode according to the net charge conversion of avidin and the SiN pore wall at different solution pH levels (Figure 1-3a). The effect of the pH on the event frequency of avidin translocation through a nanopore was experimentally determined; the change in the event frequency was due to the balance between the electroosmotic flow velocity generated by the electric double layer near SiN and the electrophoretic velocity of avidin. Likewise, Steinbock *et al.* and Fologea *et al.* demonstrated conversion of the net charge of BSA and its effect on nanopore translocation events, by shifting pH of the electrolyte above or below the isoelectric point (pI) of BSA (pI = 4.7).[3, 8] These results suggest that a change in the zeta potential of a protein and the pore wall under the influence of pH is useful for controlling the mode of translocation and the translocation rate.

① Hongsik Chae contributed to the article (ref. 20) as co-author

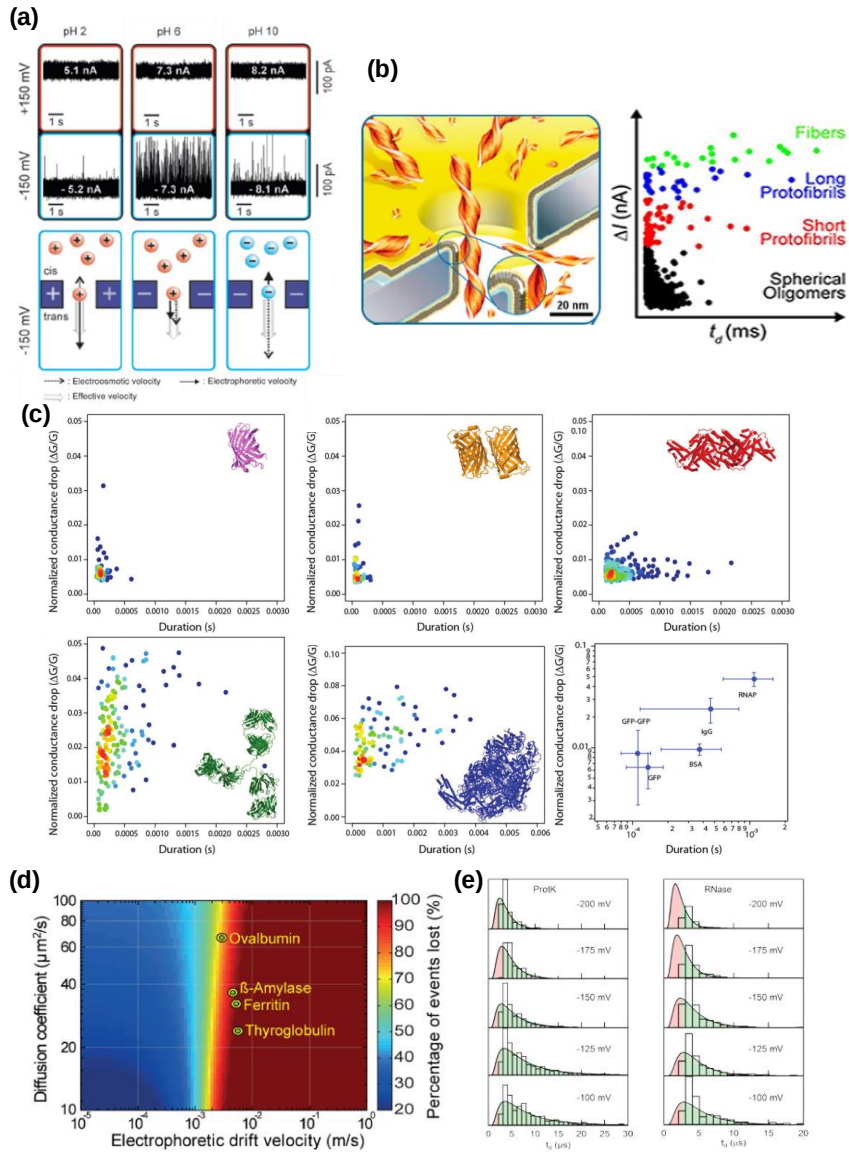

Figure 1-3. Single-molecule protein characterization using the solid-state nanopore. (a) Avidin translocation through a SiN nanopore at different pH levels in solution and corresponding charge states of avidin and SiN wall. (b) Aβ conformation analysis using a lipid bilayer-coated nanopore based on ΔI of translocation signals. (c) Scatter plots of translocation duration versus normalized conductance drop for proteins studied using the glass capillary nanopores. Each scatter plot represents translocation events of green fluorescent protein (GFP, pink), GFP–GFP dimer (FP, orange), BSA (red), IgG (green), and RNA polymerase (RNAp, navy). All the results are summarized in the rightmost graph in the second row. (d) The nanopore detection limit on the mapping of a protein expressed as the interplay of the in-pore molecular diffusivity and the electrophoretic drift velocity. (e)

Nanopore translocation time histogram of proteinase K (left) and RNase (right) at 100−200 mV, with red-shadowed regions indicating the signal loss caused by limited temporal resolution of a nanopore. The y-axis shows arbitrary units. Figure adopted from ref. 20.

1.1.1.2.2. Conformation of proteins

Another important feature of a protein that is resolvable by the solid-state nanopore is the conformation or the size of the protein. Several studies in the field of solid-state nanopore have distinguished protein conformation change before and after its full denaturation.[21-30] Without degrading the protein functionality, Yusko *et al.* identified differently sized Aβ aggregates as spherical oligomers, protofibrils, or mature fibers according to their translocation signals in the lipid-coated solid-state nanopore (Figure 1-3b).[26] They proved the feasibility of size discrimination among heterogeneous Aβ aggregates in solution using the solid-state nanopore. Moreover, the particle size characterization principle enabled profiling of the kinetic process of Aβ fibrilization by monitoring the event frequency of each Aβ aggregates. Consumption of small oligomers in the fibrillization process was reflected in a decrease in its event frequency over time, while the frequency of the translocation events for the mature fibril increased from day 0 to day 3. The trend of the protein conformation change observed using the solid-state nanopore was in agreement with the electron micrographs of Aβ taken in the same time periods.

1.1.1.2.3. Molecular weight of proteins

Li *et al.* attempted discrimination of several proteins of different sizes, with their molecular weights ranging from 14 to 465 kDa, by means of the glass nanocapillaries.[31] The protein detection using the low-noise glass-based nanopore was successful in this work. Nonetheless, the protein size could not be clearly discriminated because of too fast translocation of proteins accompanied by signal distortion by the lowpass filter. Similarly, Steinbock *et al.* also succeeded in distinguishing proteins of 12- to 480-kDa by means of glass nanocapillaries (Figure 1-3c).[8] Although they applied a 10-kHz Bessel filter to process the ionic current signals, differentiating the scatter plots of conductance drop versus dwell time for each protein was possible because they fabricated a glass nanopore with a diameter as small as the target proteins to enhance the SNR.

1.1.1.2.4. Protein-protein interactions

Arising from the detection of single proteins and protein size discrimination, analysis of protein-protein interactions (PPIs) via detection of protein-protein complexes is another branch of the protein-based application of the solid-state nanopore.[32-39] The works on the detection of protein-protein complexes based on PPIs using the solid-state nanopore are graphically presented in Figure 1-4. PPIs originate from specific binding between different proteins, which is the most important and the most basic physiological function of proteins. On the basis of this feature, Uram *et al.* observed changes in the nanopore signals due to binding of an antibody and virus (Figure 1-4a). They discriminated the signals generated by the virus (PBCV-1) and by the complex of antibodies (antiserum) with the virus; the increase of the volume of the particle after binding increased the peak amplitude. They also analyzed the binding kinetics of the antibodies and viruses quantitatively by examining the changes in the peak amplitude over time. Using the same principle, Freedman *et al.* detected the binding of HIV antigen gp120 and its antibody using the nanopore signals.[36] For more practical applications, they studied heterogeneous protein samples of the antibody+gp120 mixture, antibody+BSA mixture, antibody+gp120+BSA, and antibody+gp120+fetal bovine serum (FBS) (Figure 1-4b). They confirmed that the additional distribution of the current drop from the translocation of the antibody–gp120 complex appeared at a larger ΔI,

verifying the formation of the complex. In addition, they demonstrated that the interaction between BSA and the antibody was nonexistent by matching the current drop value observed during the biomolecule translocation for the antibody and for the antibody+BSA mixture. These studies have shown the possibility of nanopore sensors as a tool for future drug design, where complicated procedures such as molecular immobilization and labeling in the existing immunoassays are unnecessary.

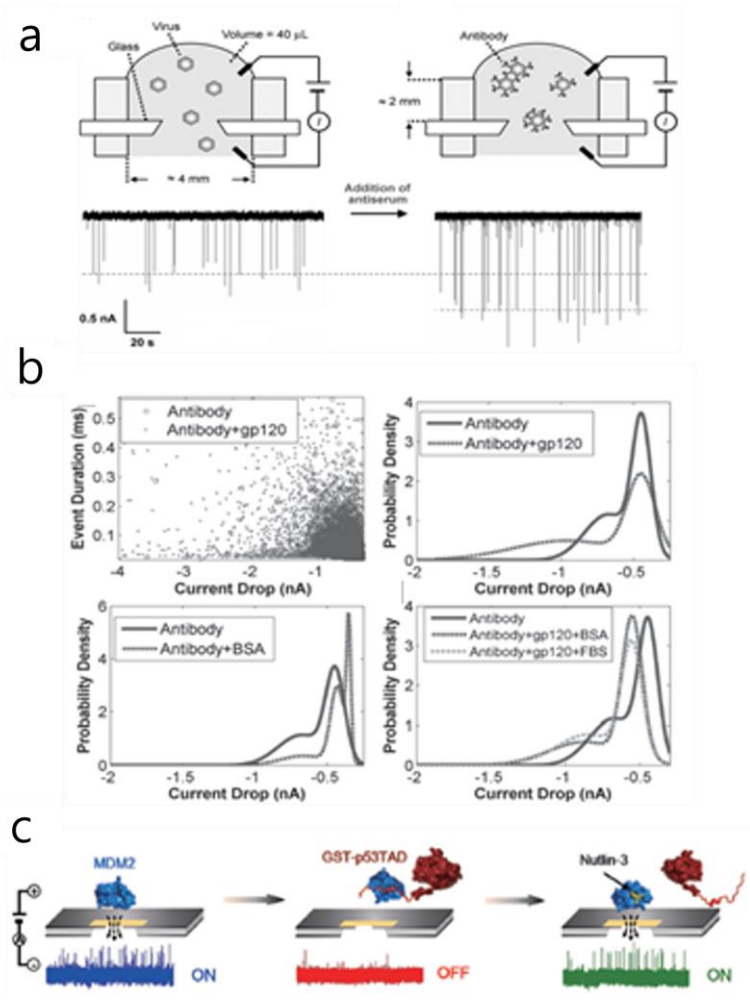

Figure 1-4. Protein–protein interaction analysis. (a) Analysis of the antibody–PBCV-1 virus interaction using the glass nanopore and resulting translocation signals. (b) Analysis of the HIV antigen gp120, an antibody, and a protein (BSA and FBS) using the nanopore according to the current drop magnitude. (c) Nanopore-based analysis of inhibition of the p53–MDM2 interaction by a drug (Nutlin-3). The cartoons on the interactions between molecules and resulting translocation signals are presented. Figure adopted from ref. 20.

1.1.2. Issues in solid-state nanopores for protein sensing

1.1.2.1. Fast translocation of protein molecules

Although numerous studies on single-protein characterization using the solid-state nanopore revealed biophysical properties of proteins, detecting the fast translocation of a protein is still limited by the insufficient temporal resolution of the measurement system. Plesa *et al.* explored the nanopore detection limit for each protein with molecular weights ranging from 6 to 660 kDa. Using a one-dimensional (1D) first-passage time-distribution model,[24, 40, 41] they calculated the event loss ratio as a function of the drift velocity of the proteins and the diffusion coefficient (Figure 1-3d). They revealed that application of the 10-kHz low-pass Bessel filter caused a severe loss of the translocation signals because of the temporal resolution limit, suggesting that an amplifier with a higher data acquisition frequency is required for protein detection.

1.1.2.2. Approaches to improve sampling rate

Larkin *et al.* employed a high bandwidth amplifier sampling the ionic current signals at a 4-MHz frequency and filtering the high-frequency signals at 250 kHz (Figure 1-3e).[6] They concluded that with the signal amplifier having the MHz bandwidth, 30–80% of the events were detected among RNase translocation events, and 70–90% of the events were detected among proteinase K (ProtK) translocations. These studies qualitatively and quantitatively indicate that proteins with molecular weight <50 kDa cross the nanopore at undetectably fast velocity and cause severe distortion in the translocation signals. Accordingly, to improve the resolution of protein translocation events in the solid-state nanopore, it is necessary to use a high-frequency amplifier and a nanopore device with low electrical noise even at high-frequency range.

Another approach to improve temporal resolution in the nanopore system was demonstrated by Shekar *et al*., by introducing the complementary metal-oxide-semiconductor (CMOS) nanopore (CNP) amplifier system.[42] The integrated CMOS nanopore system capable of temporal resolution to 100 ns. They investigate the translocation signal of 100 nucleotide (nt) single-strand DNA (ssDNA) through nanopore at 10 kHz, 200 kHz, 1 MHz, and 5 MHz filtering bandwidths (Figure 1-5). This results shows the translocation feature for ssDNA detection could be identified in sub-micro second resolution at 5 MHz filter frequency, which does not be resolved at 1

MHz bandwidth. Also, the analysis of dwell time histogram for 100 nt ssDNA translocation event obtained under relatively high voltage (900 mV) for accelerating dragging speed, they resolved the characteristic time (τ) of the data filtered at 200 kHz, 1 MHz, and 5 MHz by fitting exponential decay function ($A_1e^{-t/\tau1} + A_2e^{-t/t2}$, $\tau_1 < \tau_2$), showing $\tau_1 \sim 3.56$ μs, 2.58 μs, and 1.13 μs, for 200 kHz, 1 MHz, and 5 MHz, respectively.

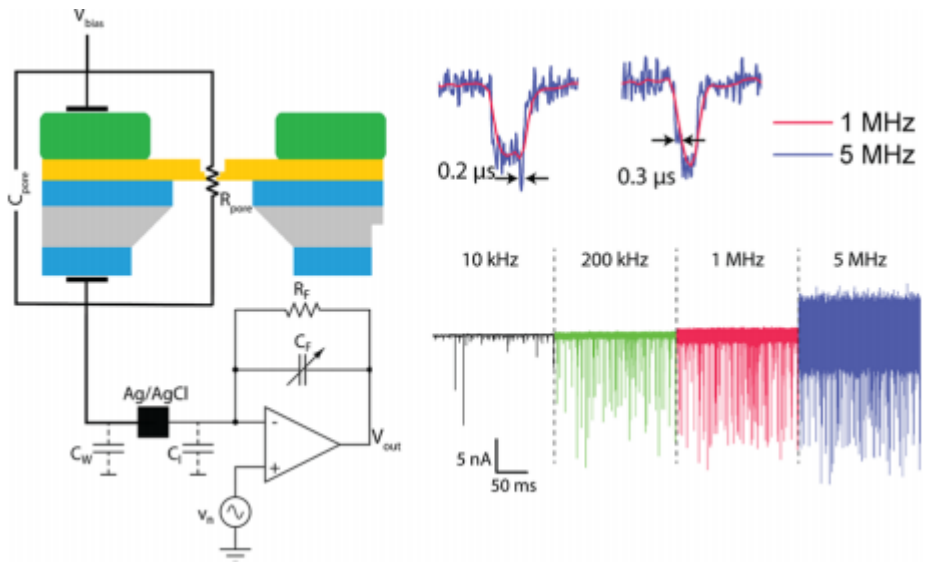

Figure 1-5. Measurement of DNA translocation using complementary metal-oxide semiconductor nanopore system with high-bandwidth filtering frequencies. Unresolved peak at 1 MHz filter frequency becomes resolved at sub-micro second level at 5 MHz. Adopted from ref. 42.

1.2. Drug screening

Drug screening is the process of evaluating the pharmacological activity and toxicity of synthetic compounds or natural products that may be candidates for new drugs. Among various therapeutic targets, antibodies show highly specific for their molecular target and exhibit stable in human serum. However, they suffer difficult in manufacturing and high cost of products. Also, the lack of oral bioavailability obstructs its development.

Nucleic acid-targeted drug discovery has advantages in high specific interaction and especially, it is stable under harsh chemical or physical treatment; however, the target site must be exposed and the short lifetime of oligonucleotide leads to degradation of the targets.

Among various therapeutic targets, the development of protein-protein interaction targeted drug discovery is challenging due to its unknown binding pocket structure and lack of natural small-molecule inhibitors.[43, 44] Due to its difficulties of identification of structure of binding sites, the development drug discovery in protein-protein interaction as a therapeutic target show less than 8% among whole drug target family.[43] Also, the difficulty of drug discovery becomes extremely high as complexity of structure of epitope increases. Thus the development of robust, ultra-fast, and high-throughput screening method is required.

1.2.1. Drug screening methods

Since protein-protein interaction and its inhibition induces change in conformation, rotational freedom, or its functionality, various technique has been developed for detecting the characteristics caused by the protein-drug interactions. For example, i) x-ray crystallography (XRC) visualizes crystal structure at atomic resolution, but provides no quantitative affinity information, ii) nuclear magnetic resonance (NMR) discriminates ligand binding to unlabeled proteins but considerable large amount of protein is required (~mg quantities)[45], iii) surface plasmon resonance (SPR) exhibits very high sensitivity, yet immobilization of target or chemical modification is inevitabble[46], iv) isothermal titration calorimetry (ITC) is very useful technique for determining thermodynamic parameters for a binary system but it requires high protein consumption and high solubility of titrated component.[47] The other technique that currently utilized in detection of protein-protein interaction and protein-drug interaction are summarized in Table 1-1.

Table 1-1. Summary of currently used methods for detecting protein-protein interaction and protein-drug interactions.

Technique or method	Strengths	Limitations
X-ray Crystallography (XRC)	• Direct visualization at atomic resolution of target-ligand interactions	• No quantitative affinity information
Nuclear Magnetic Resonance (NMR)	• Confirmation of ligand binding to unlabeled proteins of any size	• Considerably large amounts of protein required (~tens of mg quantity)
Surface Plasmon Resonance (SPR)	• High sensitivity allows analysis of fragments	• Requires immobilization of functional target with high stability over time
Isothermal Titration Calorimetry (ITC)	• Direct determination of the effect of a ligand on the thermal stability of a protein	• High protein consumption • Only applied for binding event with enthalpic component
Mass Spectrometry (MS)	• Direct visualization of complex formation • High sensitivity • Accurate mass measurement • No labeling required	• Desalted sample is required • Unspecific binding causes difficult detection for low-affinity binders
Quartz Crystal Microbalance (QCM)	• Direct time-resolved determination of interaction	• Immobilization is required for the functional target with high stability over time

1.3. Solid-state nanopores for drug screening platform

1.3.1. Nucleic acid and small-molecule interaction

Solid-state nanopores are emerging ultra-sensitive single-molecule sensors that have been utilized in detection of biomolecules such as nucleic acids or proteins.[48] In addition to single-molecule detection, research on solid-state nanopores have been expanded to analysis on molecular interactions as a diagnostic platform. For example, interaction between nucleic acid and small molecule have been explored by identifying small-molecule binding site on nucleic acid from characteristic ionic current signals that arise from nanopore translocation of nucleic acid strand with local small-molecule binding site.[49-55] Based on the principle of nanopore measurement which records the change in ionic current caused by the passing molecule temporarily blocking the nanopore, the increased volume at the position or binding site of the target molecule could be successfully recognized. For instant, Yu *et al.* have identified the binding position of zinc finger protein on double-stranded DNA (dsDNA) by recognizing additional current drop in a single molecule translocation signal.[51] The binding of zinc finger protein at symmetric (1-to-1) or asymmetric position (2-to-5) of designed DNA containing the specific binding site for the zinc finger protein causes additional volume expansion, thereby results in additional peak in the single molecule translocation signal. The identical peak position of the additional peak with the designed binding site of the zinc finger protein along the DNA

molecule reveals that the specific binding of protein could be detected using solid-state nanopores.

Although solid-state nanopores are high-resolution measurement tool that have been utilized in identification of binding of a small molecule by detecting characteristic current signature, the quantitative estimation of molecular interaction is required to develop the solid-state nanopore as a diagnostic platform. For the quantitative evaluation, researchers have investigated the binding affinity of interacting molecules by using solid-state nanopores. For example, Wanunu *et al.* have demonstrated the nanopore titration of three different intercalating dye molecules (ethidium bromide, propidium, and ethidium homodimer) with each different binding affinities into a 400 bp dsDNA fragments.[50] By increasing the dye concentration, they monitored increased current drop amplitude of translocation signal of dye-bound DNA. This results show an excellent agree with fluorescence titration experiment, but the direct estimation using nanopore data was not demonstrated.

Another result of nanopore evaluation of binding affinity for small molecule with nucleic acid have been reported by Wanunu *et al.*, demonstrating direct titration from change in current drop amplitude of nanopore signals.[52] Based on the change in current drop upon addition of paromomycin (PM), which binds to the A-site RNA as a aminoglycoside, they monitored the newly appeared current drop population. Since the newly appearing population is not clearly distinguishable from the population in the drug-free RNA,

however, they the formulated the binding fraction by dividing mean current drop (ΔI_{Norm}) by mean current drop at high concentration of PM (ΔI_{Max}). By assuming 1:1 binding for the A-site RNA with PM, and the total drug concentration is approximately equal to the free drug concentration[56], the dissociation constant (K_d) can be estimated by fitting the simplified binding curve

$$f = \frac{[\text{Drug}]}{[\text{Drug}] + K_d} \quad (1)$$

where f is binding fraction,[46] is concentration of drug molecule, and K_d is dissociation constant, respectively.

1.3.2. Protein-protein interaction inhibitor screening

While there are remarkable accomplishments in nucleic acids, only a few results have been reported for titration of drug into protein complex or protein-protein interactions. Protein-protein interactions (PPIs) are involved in metabolisms, cell signaling, and gene regulatory networks. Thus mediating PPI by drug molecule is key target for molecular studies for human diseases.[57] Also, due to extremely high specificity of the interaction, PPIs are highlighted as an attractive drug screening target.[44] While nucleic acids exhibit linear conformation with uniformly charged structure, proteins have variety of structures with heterogeneous charge distribution. Since protein has 3-dimentional structure, the orientation varies during translocation, which might cause inconsistent current drop. Since estimating binding affinity by current drop change is limited to the molecules that i) measured in consistent current drop for drug-free state, and ii) cause a volume expansion upon ligand binding, the quantitative evaluation of dissociation equilibrium in protein-small-ligand interface is challenging.

Recently, Kwak *et al.*, have demonstrated protein-protein interaction of cancer target protein of p53 and MDM2, as well as its inhibition by small molecule inhibitor (Nutlin-3) through nanopore detection.[19] Based on charge inversion of MDM2 upon interaction between p53 (K_d ~0.6 μM), they monitored the significantly reduced event frequency of MDM2 translocation. Also, the recovered event frequency was detected by addition of Nutlin-3 (K_d ~0.1 μM)[58, 59]. This is a remarkable result that resolving translocation

event of such small cancer target biomarkers (<15 kDa) could be demonstrated by low-noise solid-state nanopores. Although the authors demonstrated the protein-protein interaction and its inhibition by using a noble method, this result still suffered from lack of resolution of detection system (10 kHz filter and 250 kHz sampling rate). Since translocation speed of such a small protein exhibits extremely fast, the dwell time of traversing time shows 1-1000 μs. Thus, there is a probability of severe data distortion in the translocation signal of p53 and MDM2.

By showing the unrestored event frequency of MDM2 upon addition of ABT-737, the authors probed that the interaction of p53 and MDM2 was specifically inhibited by Nutlin-3 through an experiment of a negative control (ABT-737). However, it is still limited that the charge inversion must be involved upon protein-protein interaction, as well as charge conservation of MDM2 by inhibitor addition.

In the next chapter, my demonstration of protein-protein interaction and its inhibition is introduced by overcoming the limitation of charge state of proteins, as well as the temporal resolution of measurement system.

1.4. References

1. Wanunu, M. J. P. o. l. r., Nanopores: A journey towards DNA sequencing. **2012,** *9* (2), 125-158.

2. Firnkes, M.; Pedone, D.; Knezevic, J.; Doblinger, M.; Rant, U., Electrically Facilitated Translocations of Proteins through Silicon Nitride Nanopores: Conjoint and Competitive Action of Diffusion, Electrophoresis, and Electroosmosis. *Nano Lett* **2010,** *10* (6), 2162-2167.

3. Fologea, D.; Ledden, B.; McNabb, D. S.; Li, J., Electrical characterization of protein molecules by a solid-state nanopore. *Appl Phys Lett* **2007,** *91* (5), 539011-539013.

4. Han, A.; Schürmann, G.; Mondin, G.; Bitterli, R. A.; Hegelbach, N. G.; de Rooij, N. F.; Staufer, U., Sensing protein molecules using nanofabricated pores. *Applied Physics Letters* **2006,** *88* (9), 093901.

5. Kannam, S. K.; Kim, S. C.; Rogers, P. R.; Gunn, N.; Wagner, J.; Harrer, S.; Downton, M. T., Sensing of protein molecules through nanopores: a molecular dynamics study. *Nanotechnology* **2014,** *25* (15), 155502.

6. Larkin, J.; Henley, R. Y.; Muthukumar, M.; Rosenstein, J. K.; Wanunu, M., High-Bandwidth Protein Analysis Using Solid-State Nanopores. *Biophysical journal* **2014,** *106* (3), 696-704.

7. Plesa, C.; Kowalczyk, S. W.; Zinsmeester, R.; Grosberg, A. Y.; Rabin, Y.; Dekker, C., Fast translocation of proteins through solid state

nanopores. *Nano Lett* **2013,** *13* (2), 658-663.

8. Steinbock, L. J.; Krishnan, S.; Bulushev, R. D.; Borgeaud, S.; Blokesch, M.; Feletti, L.; Radenovic, A., Probing the size of proteins with glass nanopores. *Nanoscale* **2014,** *6* (23), 14380-7.

9. Wu, L. Z.; Liu, H.; Zhao, W. Y.; Wang, L.; Hou, C. R.; Liu, Q. J.; Lu, Z. H., Electrically facilitated translocation of protein through solid nanopore. *Nanoscale Res Lett* **2014,** *9* (1), 1-10.

10. Apparatus and method for measuring a dividing particle size of a particulate system. Google Patents: 1971.

11. Sutherland, T. C.; Long, Y.-T.; Stefureac, R.-I.; Bediako-Amoa, I.; Kraatz, H.-B.; Lee, J. S. J. N. l., Structure of peptides investigated by nanopore analysis. **2004,** *4* (7), 1273-1277.

12. Uram, J. D.; Ke, K.; Hunt, A. J.; Mayer, M., Submicrometer Pore-Based Characterization and Quantification of Antibody–Virus Interactions. *Small* **2006,** *2* (8-9), 967-972.

13. Freedman, K. J.; Bastian, A. R.; Chaiken, I.; Kim, M. J., Solid-State Nanopore Detection of Protein Complexes: Applications in Healthcare and Protein Kinetics. *Small* **2013,** *9* (5), 750-759.

14. Tavassoly, O.; Kakish, J.; Nokhrin, S.; Dmitriev, O.; Lee, J. S., The use of nanopore analysis for discovering drugs which bind to α-synuclein for treatment of Parkinson's disease. *European journal of medicinal chemistry* **2014,** *88*, 42-54.

15. Yusko, E. C.; Prangkio, P.; Sept, D.; Rollings, R. C.; Li, J.;

Mayer, M., Single-particle characterization of Aβ oligomers in solution. *ACS nano* **2012,** *6* (7), 5909-5919.

16. Plesa, C.; Kowalczyk, S. W.; Zinsmeester, R.; Grosberg, A. Y.; Rabin, Y.; Dekker, C., Fast translocation of proteins through solid state nanopores. *Nano letters* **2013,** *13* (2), 658-663.

17. Larkin, J.; Henley, R. Y.; Muthukumar, M.; Rosenstein, J. K.; Wanunu, M., High-bandwidth protein analysis using solid-state nanopores. *Biophysical journal* **2014,** *106* (3), 696-704.

18. Kennedy, E.; Dong, Z.; Tennant, C.; Timp, G., Reading the primary structure of a protein with 0.07 nm3 resolution using a subnanometre-diameter pore. *Nature Nanotechnology* **2016**.

19. Kwak, D. K.; Chae, H.; Lee, M. K.; Ha, J. H.; Goyal, G.; Kim, M. J.; Kim, K. B.; Chi, S. W., Probing the Small-Molecule Inhibition of an Anticancer Therapeutic Protein-Protein Interaction Using a Solid-State Nanopore. *Angewandte Chemie International Edition* **2016,** *55* (19), 5713-5717.

20. Lee, K.; Park, K. B.; Kim, H. J.; Yu, J. S.; Chae, H.; Kim, H. M.; Kim, K. B. J. A. M., Recent Progress in Solid-State Nanopores. **2018,** *30* (42), 1704680.

21. Freedman, K. J.; Haq, S. R.; Edel, J. B.; Jemth, P.; Kim, M. J., Single molecule unfolding and stretching of protein domains inside a solid-state nanopore by electric field. *Sci Rep* **2013,** *3*, 1638.

22. Freedman, K. J.; Jurgens, M.; Prabhu, A.; Ahn, C. W.; Jemth,

P.; Edel, J. B.; Kim, M. J., Chemical, Thermal, and Electric Field Induced Unfolding of Single Protein Molecules Studied Using Nanopores. *Analytical chemistry* **2011,** *83* (13), 5137-5144.

23. Oukhaled, A.; Cressiot, B.; Bacri, L.; Pastoriza-Gallego, M.; Betton, J. M.; Bourhis, E.; Jede, R.; Gierak, J.; Auvray, L.; Pelta, J., Dynamics of Completely Unfolded and Native Proteins through Solid-State Nanopores as a Function of Electric Driving Force. *ACS Nano* **2011,** *5* (5), 3628-3638.

24. Talaga, D. S.; Li, J., Single-molecule protein unfolding in solid state nanopores. *J Am Chem Soc* **2009,** *131* (26), 9287-97.

25. Cressiot, B.; Oukhaled, A.; Patriarche, G.; Pastoriza-Gallego, M.; Betton, J. M.; Auvray, L.; Muthukumar, M.; Bacri, L.; Pelta, J., Protein Transport through a Narrow Solid-State Nanopore at High Voltage: Experiments and Theory. *ACS Nano* **2012,** *6* (7), 6236-6243.

26. Yusko, E. C.; Prangkio, P.; Sept, D.; Rollings, R. C.; Li, J. L.; Mayer, M., Single-Particle Characterization of A beta Oligomers in Solution. *ACS Nano* **2012,** *6* (7), 5909-5919.

27. Japrung, D.; Dogan, J.; Freedman, K.; Nadzeyka, A.; Bauerdick, S.; Albrecht, T.; Kim, M. J.; Jemth, P.; Edel, J. B., Single-Molecule Studies of Intrinsically Disordered Proteins Using Solid-State Nanopores. *Analytical chemistry* **2013,** *85* (4), 2449-2456.

28. Martyushenko, N.; Bell, N. A.; Lamboll, R. D.; Keyser, U. F., Nanopore analysis of amyloid fibrils formed by lysozyme aggregation.

Analyst **2015,** *140* (14), 4882-6.

29. Hu, R.; Diao, J.; Li, J.; Tang, Z.; Li, X.; Leitz, J.; Long, J.; Liu, J.; Yu, D.; Zhao, Q., Intrinsic and membrane-facilitated alpha-synuclein oligomerization revealed by label-free detection through solid-state nanopores. *Sci Rep* **2016,** *6*, 20776.

30. Yusko, E. C.; Bruhn, B. R.; Eggenberger, O. M.; Houghtaling, J.; Rollings, R. C.; Walsh, N. C.; Nandivada, S.; Pindrus, M.; Hall, A. R.; Sept, D.; Li, J.; Kalonia, D. S.; Mayer, M., Real-time shape approximation and fingerprinting of single proteins using a nanopore. *Nature nanotechnology* **2016**.

31. Li, W.; Bell, N. A.; Hernandez-Ainsa, S.; Thacker, V. V.; Thackray, A. M.; Bujdoso, R.; Keyser, U. F., Single protein molecule detection by glass nanopores. *ACS Nano* **2013,** *7* (5), 4129-34.

32. Uram, J. D.; Ke, K.; Hunt, A. J.; Mayer, M., Submicrometer pore-based characterization and quantification of antibody-virus interactions. *Small* **2006,** *2* (8-9), 967-72.

33. Uram, J. D.; Ke, K.; Hunt, A. J.; Mayer, M., Label-free affinity assays by rapid detection of immune complexes in submicrometer pores. *Angew Chem Int Ed Engl* **2006,** *45* (14), 2281-5.

34. Han, A.; Creus, M.; Schürmann, G.; Linder, V.; Ward, T. R.; de Rooij, N. F.; Staufer, U., Label-free detection of single protein molecules and protein− protein interactions using synthetic nanopores. *Analytical chemistry* **2008,** *80* (12), 4651-4658.

35. Wei, R.; Gatterdam, V.; Wieneke, R.; Tampe, R.; Rant, U., Stochastic sensing of proteins with receptor-modified solid-state nanopores. *Nature nanotechnology* **2012,** *7* (4), 257-63.

36. Freedman, K. J.; Bastian, A. R.; Chaiken, I.; Kim, M. J., Solid-state nanopore detection of protein complexes: applications in healthcare and protein kinetics. *Small* **2013,** *9* (5), 750-9.

37. Tiwari, P. B.; Astudillo, L.; Miksovska, J.; Wang, X.; Li, W.; Darici, Y.; He, J., Quantitative study of protein-protein interactions by quartz nanopipettes. *Nanoscale* **2014,** *6* (17), 10255-63.

38. Kwak, D. K.; Chae, H.; Lee, M. K.; Ha, J. H.; Goyal, G.; Kim, M. J.; Kim, K. B.; Chi, S. W., Probing the Small-Molecule Inhibition of an Anticancer Therapeutic Protein-Protein Interaction Using a Solid-State Nanopore. *Angew Chem Int Ed Engl* **2016,** *55* (19), 5713-7.

39. Takakura, T.; Yanagi, I.; Goto, Y.; Ishige, Y.; Kohara, Y., Single-molecule detection of proteins with antigen-antibody interaction using resistive-pulse sensing of submicron latex particles. *Appl Phys Lett* **2016,** *108* (12), 123701.

40. Li, J.; Talaga, D. S., The distribution of DNA translocation times in solid-state nanopores. *J Phys Condens Matter* **2010,** *22* (45), 454129.

41. Ling, D. Y.; Ling, X. S., On the distribution of DNA translocation times in solid-state nanopores: an analysis using Schrodinger's first-passage-time theory. *J Phys Condens Matter* **2013,** *25* (37), 375102.

42. Shekar, S.; Niedzwiecki, D. J.; Chien, C.-C.; Ong, P.;

Fleischer, D. A.; Lin, J.; Rosenstein, J. K.; Drndić, M.; Shepard, K. L., Measurement of DNA translocation dynamics in a solid-state nanopore at 100 ns temporal resolution. *Nano letters* **2016,** *16* (7), 4483-4489.

43. Eder, J.; Sedrani, R.; Wiesmann, C. J. N. R. D. D., The discovery of first-in-class drugs: origins and evolution. **2014,** *13* (8), 577.

44. Wells, J. A.; McClendon, C. L. J. N., Reaching for high-hanging fruit in drug discovery at protein–protein interfaces. **2007,** *450* (7172), 1001.

45. Pellecchia, M.; Bertini, I.; Cowburn, D.; Dalvit, C.; Giralt, E.; Jahnke, W.; James, T. L.; Homans, S. W.; Kessler, H.; Luchinat, C.; Meyer, B.; Oschkinat, H.; Peng, J.; Schwalbe, H.; Siegal, G., Perspectives on NMR in drug discovery: a technique comes of age. *Nat Rev Drug Discov* **2008,** *7* (9), 738-45.

46. Cooper, M. A. J. N. r. D. d., Optical biosensors in drug discovery. **2002,** *1* (7), 515.

47. Ladbury, J. E.; Klebe, G.; Freire, E., Adding calorimetric data to decision making in lead discovery: a hot tip. *Nat Rev Drug Discov* **2010,** *9* (1), 23-7.

48. Dekker, C., Solid-state nanopores. *Nat Nanotechnol* **2007,** *2* (4), 209-15.

49. Yang, W.; Restrepo-Perez, L.; Bengtson, M.; Heerema, S. J.; Birnie, A.; van der Torre, J.; Dekker, C., Detection of CRISPR-dCas9 on DNA with Solid-State Nanopores. *Nano Lett* **2018,** *18* (10), 6469-6474.

50. Wanunu, M.; Sutin, J.; Meller, A., DNA Profiling Using Solid-

State Nanopores: Detection of DNA-Binding Molecules. *Nano Letters* **2009,** *9* (10), 3498-3502.

51. Yu, J. S.; Lim, M. C.; Huynh, D. T. N.; Kim, H. J.; Kim, H. M.; Kim, Y. R.; Kim, K. B., Identifying the Location of a Single Protein along the DNA Strand Using Solid-State Nanopores. *Acs Nano* **2015,** *9* (5), 5289-5298.

52. Wanunu, M.; Bhattacharya, S.; Xie, Y.; Tor, Y.; Aksimentiev, A.; Drndic, M., Nanopore analysis of individual RNA/antibiotic complexes. *ACS Nano* **2011,** *5* (12), 9345-53.

53. Bell, N. A. W.; Keyser, U. F., Specific Protein Detection Using Designed DNA Carriers and Nanopores. *Journal of the American Chemical Society* **2015,** *137* (5), 2035-2041.

54. Japrung, D.; Bahrami, A.; Nadzeyka, A.; Peto, L.; Bauerdick, S.; Edel, J. B.; Albrecht, T., SSB Binding to Single-Stranded DNA Probed Using Solid-State Nanopore Sensors. *J Phys Chem B* **2014,** *118* (40), 11605-11612.

55. Smeets, R.; Kowalczyk, S. W.; Hall, A.; Dekker, N.; Dekker, C. J. N. l., Translocation of RecA-coated double-stranded DNA through solid-state nanopores. **2008,** *9* (9), 3089-3095.

56. Shortridge, M. D.; Hage, D. S.; Harbison, G. S.; Powers, R., Estimating protein− ligand binding affinity using high-throughput screening by NMR. *Journal of combinatorial chemistry* **2008,** *10* (6), 948-958.

57. Gonzalez, M. W.; Kann, M. G., Chapter 4: Protein interactions and

disease. *Plos Comput Biol* **2012,** *8* (12), e1002819.

58. Vassilev, L. T.; Vu, B. T.; Graves, B.; Carvajal, D.; Podlaski, F.; Filipovic, Z.; Kong, N.; Kammlott, U.; Lukacs, C.; Klein, C., In vivo activation of the p53 pathway by small-molecule antagonists of MDM2. *Science* **2004,** *303* (5659), 844-848.

59. Fesik, S. W., Promoting apoptosis as a strategy for cancer drug discovery. *Nature Reviews Cancer* **2005,** *5* (11), 876.

Chapter 2. Solid-State Nanopore Analysis on Conformation Change of p53TAD–MDM2 Fusion Protein Induced by Protein–Protein Interaction[1②]

② Hongsik Chae and Dong-Kyu Kwak contributed equally to this work as a first author

2.1. Introduction

Protein-protein interactions (PPIs) are involved in crucial regulatory processes of cell signaling such as cell division, programmed cell death, and tumorigenesis. Therefore, the regulation of PPIs have been actively investigated as emerging therapeutic targets for human diseases.[2] Among traditional drug targets, enzymes and therapeutic antibodies have been primarily used for drug development. However, the development of enzyme-targeted drugs has been hampered by off-target side-effects,[3] and the development of antibodies has suffered from difficulties in developing an economically viable manufacturing process.[4] Therefore, an expansion of druggable targets is urgently needed to accelerate drug development. In this respect, PPIs have attractive advantages compared to other methods to identify drug molecules owing to their broad protein-protein interfaces and the extremely high specificity of the interaction. In particular, the discovery of PPI inhibitors that are able to specifically interfere with the regulatory roles of PPIs is a promising strategy to fulfill unmet needs in pharmaceutical and medical industries.[5]

To efficiently discover proper PPI inhibitors, development of high-throughput screening (HTS) processes of the drug molecule is essential. However, development of HTS technologies against PPI targets remains challenging in spite of recent advances in drug screening processes. To date, several techniques such as nuclear magnetic resonance (NMR),[6] surface

plasmon resonance (SPR)[7], fluorescence polarization (FP), and fluorescence resonance energy transfer (FRET)[8] have been developed for PPI analysis and drug screening[9, 10]. However, NMR requires a large amount of sample and SPR exhibits low sensitivity for detection of small-molecule binding.[11] For PPI detection using FP and FRET, the immobilization of proteins or labeling of fluorophores is indispensable for detection.[8] Undoubtedly, the development of a fast and label-free detection technique is required for efficient discovery of drug molecules based on PPIs.

Recently, solid-state nanopore has been highlighted as an ultra-sensitive and native-state measurement technique at the single-molecule level[12, 13] and is applicable to characterize protein-protein interactions,[14-18] folding/unfolding of biomolecules,[19-22] and conformational changes.[23] For instance, Freedman *et al.* detected the gp120-antibody interaction from a larger current drop signal (ΔI) in solid-state nanopore measurement resulting from the gp120-antibody interaction forming a complex with a larger volume.[24] In addition, Yusko *et al*. reported the aggregation of β-amyloid protein monomers to form a fibrillar structure, detected by current drop and dwell time changes, as well as changes in event frequencies.[25] Waduge *et al.* also recently reported the detection of two different structures of calmodulin complex induced by calcium ions using high-bandwidth nanopore measurement.[26] The authors designed a system in which the two globular domain is connected by a flexible linker that forms either a single or double globular

domains depending on Ca^{2+} addition, as these ions bind to calmodulin and inhibit its interaction. The authors noted that the extended form of the calmodulin shows a longer dwell time and larger current drop than the one forming a single globular structure.

In chapter 1.3.2, the interaction between the p53 transactivation domain (p53TAD) and mouse double minute 2 (MDM2) as well as its inhibition by nutlin-3 using solid-state nanopores is reported.[27] p53 is a tumor suppressor protein that induces cell cycle arrest and apoptosis in response to stress signals such as DNA damage. MDM2 is known to negatively regulate the tumor suppressive activity of p53 via a direct interaction with p53TAD (K_d = ~ 600 nM).[28, 29] It is well known that nutlin-3 binds to MDM2 by mimicking the α-helical conformation of the 15-residue p53TAD peptide (residues 15-29), thus preventing the binding of p53TAD and MDM2.[30, 31] In our previous reports, we detected the interaction between p53TAD and MDM2 by changes in translocation event frequency. Namely, positively charged MDM2 protein (isoelectric point; pI = 9.0) is driven through a nanopore by the applied negative potential. However, when a MDM2/p53TAD complex forms, the overall charge state of the complex changes to negative as a result of charge masking by the negatively charged p53TAD (pI = 3.6). Therefore, this protein complex is not driven through a nanopore by the applied negative potential. The addition of nutlin-3 liberates MDM2 from the MDM2/p53TAD complex, allowing the translocation of MDM2 through a

nanopore under the negative potential.

In the previous chapter, we demonstrated that solid-state nanopore can be a valuable platform for screening drug molecules by monitoring the changes of translocation event frequency resulted from charge reversal as a result of PPI. However, this concept has a serious limitation to apply to a variety of PPI target since proteins involving the interaction should have different charge types (positive or negative). In this chapter, we aimed to develop a novel screening method for detecting PPI inhibitors using solid-state nanopores that can be applied to various PPI targets, without the need of charge reversal of the interacting proteins.

2.2. Experimental details

Nanopore experiment

100 nm-thick low-stress LPCVD SiN_x was deposited on 500 μm thick Si substrate. To fabricate free-standing 2x2 mm^2 window of SiN_x membrane, photolithography and reactive ion etching process was performed, followed by KOH wet etching on 5x5 mm^2 Si chip. The SiN_x membrane was transferred onto separately prepared quartz substrate, which is fabricated as previously described,[25] then the membrane was etched by CF_4 plasma to a desirable thickness (CF_4 40 sccm, 0.05 Torr, 50 W, etch rate ~ 30 nm/min). The nanopore was drilled into the SiN_x membrane using focused electron beam using TEM. Prior to use, the fabricated nanopore device was treated with oxygen plasma (15 mA, 0.20 mbar) for 2 minutes before assemble into the custom made Teflon cell with PDMS gaskets to seal solution leaking. 1 M KCl in 1×PBS buffer (pH=7.4) was filled the *cis* and *trans* chambers. After that, the assembled cell was placed in a Faraday cage. In all experiments, MLP concentration was fixed to 100 nM and introduced in the *cis* chamber. Translocation experiments were conducted under 200 mV potential across the membrane using Ag/AgCl electrode. Data were collected using Chimera VC 100 (Chimera Instruments, USA) with sampling rate of 4.16 MHz (500 kHz low-pass Bessel filter). Translocation event were analyzed by using python 2.7 based program “pythion”

(Developed in Wanunu group), Clampfit 10.4 and described using OriginPro 8 software.

Expression and purification of proteins (Courtesy of KRIBB)[③]

The DNA construct encoding MLP fusion protein (MDM2 (residues 3-109)-linker-p53TAD (residues 1-73)-GST) was cloned into the pET-21a vector. The MLP construct includes a linker composed of 16 residue-long ($(GGGS)_4$) between the C-terminus of MDM2 and the N-terminus of p53TAD. The MLP protein was overexpressed in *Escherchia coli* Rosetta™ 2 by induction with 0.5 mM isopropyl-β-D-thiogalactoside (IPTG) at the OD_{600} of 0.7. After IPTG induction, cells were grown at 20 °C for 12 hours in LB or M9 minimal media. The MLP protein was purified using GST affinity chromatography (GSTrap™, GE healthcare), anion exchange chromatography (Hitrap™ Q, GE healthcare), and gel-filtration chromatography (HiLoad® 16/600 Superdex® 75pg, GE healthcare). For NMR experiments, ^{15}N-labeled MLP protein was expressed in M9 minimal media containing ^{15}N-NH_4Cl and purified as described above. The Nutlin-3 was purchased from Cayman Chemical Inc.

③ Dr. Seung-Wook Chi and Dong-Kyu Kwak in Korea Research Institute of Bioscience and Bioengineering (KRIBB) (swchi@kribb.re.kr, dikay@kribb.re.kr)

NMR spectroscopy (Courtesy of LRIBB)④

All NMR spectra were acquired in a Bruker 900 MHz spectrometer equipped with a cryogenic probe at KBSI (Ochang, Republic of Korea). The 2D ^{15}N-^{1}H HSQC spectra of MLP were obtained at 298 K in the absence or presence of Nutlin-3. The MLP protein of 100 μM was treated with Nutlin-3 at a molar ratio of 1:5. All the NMR data were processed using the NMRPipe/NMRDraw[32] and SPARKY softwares.

④ Dr. Seung-Wook Chi and Dong-Kyu Kwak in Korea Research Institute of Bioscience and Bioengineering (KRIBB) (swchi@kribb.re.kr, dikay@kribb.re.kr)

2.3. Results and discussion

We first designed a fusion protein complex MLP (MDM2-linker-p53TAD, 48.5 kDa, pI = 5.18), which includes a relatively large glutathione-S-transferase (GST-p53TAD, pI = 4.8) tag at the C-terminus of p53, where MDM2 and p53TAD are connected by a 16 amino acid long linker ($(GGGS)_4$) to induce a conformational change between MLP and MLP-Nutlin-3 complex. MLP shows a closed form, globular shape conformation as shown in Figure 2-1a (left). The addition of Nutlin-3 disrupts the interaction between p53TAD and MDM2 owing to its relatively high binding affinity with MDM2 (K_d = ~100 nM).[31] Thus, GST-p53TAD is released from MDM2, which changes MLP structure from a closed globular form to a dumbbell-like open form (tMLP) as shown in Figure 2-1a (right).

In these experiments, we utilized SiN_x nanopores with a highly insulating dielectric substrate[33] coupled with a high frequency amplifier (4.16 MHz) to improve the signal-to-noise ratio and temporal resolution of our detection system. We expected two types of translocation signals as is schematically shown in Figure 2-1b. Because the translocation signature of a single molecule event reflects the detail structure of protein complex, the nanopore signal of MLP is expected to be a single peak (type I), whereas tMLP is expected to have a double-peak signal (type II) even though their overall volume is the same.

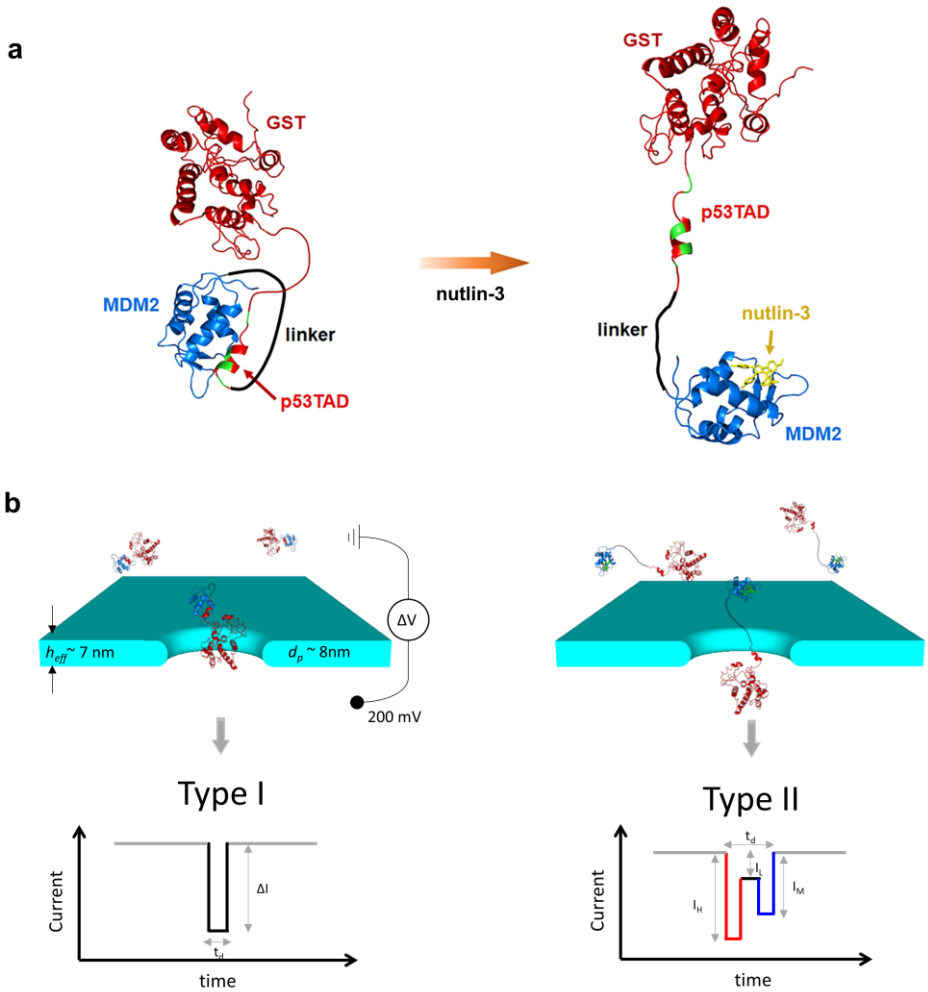

Figure 2-1. Illustration of a nanopore detection. (a) A molecular model for free and Nutlin-3-bound MLP fusion protein. GST, MDM2, and Nutlin-3 are colored in red, blue, and yellow, respectively. (b) Schematic of a nanopore detection where MLP traverses through a silicon nitride (SiN) pore with effective thickness h_{eff} = 7 nm and pore diameter d_{p} = 8 nm (not to scale). Left, single-spike signal expected from the globular structure (type I). Inhibition of p53TAD/MDM2 interaction by Nutlin-3 elongates the linker to transform MLP into a dumbbell-like structure. Right, expected distinctive double-peak nanopore signal from tMLP translocation (type II).

2.3.1. Nuclear magnetic resonance (NMR) result of p53TAD and MDM2 interaction

Prior to nanopore detection, Dr. Seung-Wook Chi and Dong-Kyu Kwak (research group in Korea Research Institute of Bioscience and Bioengineering, KRIBB) examined the PPI between MDM2 and p53TAD in a single fusion protein frame of MLP using NMR spectroscopy (Figure 2-2). The 2D ^{15}N-^{1}H heteronuclear single quantum correlation (HSQC) spectra of ^{15}N-labeled MLP were acquired in the absence or presence of Nutlin-3. In the absence of Nutlin-3, the 2D HSQC spectrum showed the ^{15}N-^{1}H crosspeaks mainly from the p53TAD region of MLP. Unlike in free p53TAD,[34] ^{15}N-^{1}H crosspeaks from the MDM2-binding residues in p53TAD of MLP (p53TAD residues 15-29, colored green in Figure 2-1a) were not observed owing to severe line-broadening by MDM2 binding. This line broadening of crosspeaks indicates that MLP retains the PPI between MDM2 and p53TAD. In contrast, we found a noticeable recovery of several NMR crosspeaks of MLP after the addition of Nutlin-3. The NMR resonance assignments revealed that the restored residues (residues 18, 20, 23, 28, and 29) are predominantly located in the MDM2-binding site of p53TAD in MLP, indicating that Nutlin-3 disrupts the PPI between MDM2 and p53TAD as expected, thereby inducing a conformational change in MLP.

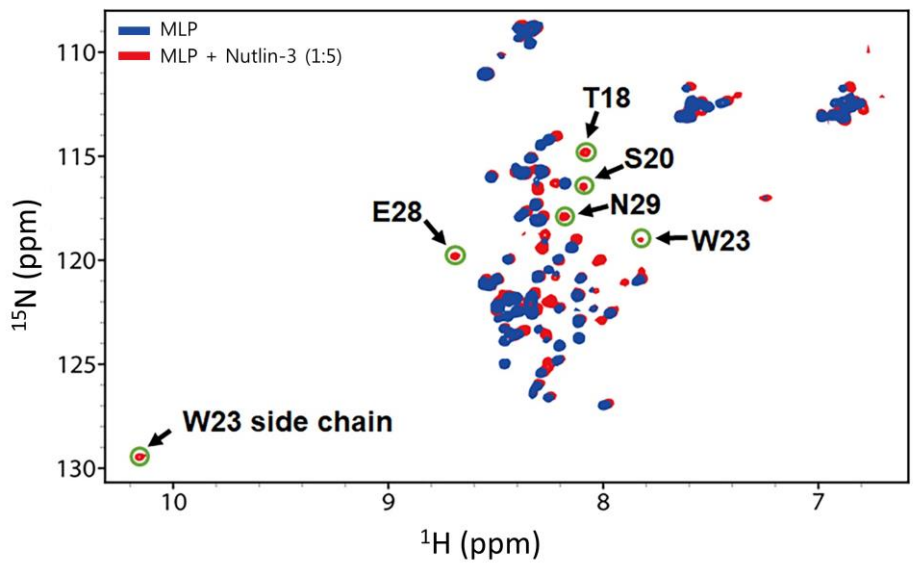

Figure 2-2. ^{15}N–^{1}H HSQC spectra of MLP with and without Nutlin-3. Crosspeaks of free (blue) and Nutlin-3-bound MLP (red) are shown. MLP was treated with Nutlin-3 at the molar ratio of 1:5. Green circles and arrows indicate the recovered crosspeaks after addition of Nutlin-3. Data provided by KRIBB (Dr. Seung-Wook Chi's group)

2.3.2. Nanopore detection of the p53TAD and MDM2 interaction with and without Nutlin-3 drug molecule

For the nanopore experiments, 1 M KCl in 1×PBS buffer solution (pH = 7.4) was filled in both the *cis* and *trans* chambers and 200 mV of electric potential was applied across the membrane to drag negatively charged MLP toward the nanopores. The protein samples were prepared by incubating MLP protein with increasing molar ratios of Nutlin-3 to MLP of zero-fold (free), 1-fold (1:1), 5-fold (1:5), and 10-fold (1:10) for 2 h. A typical I-V curve of the nanopore is presented in Figure 2-3a. The schematic structure and electron micrograph of our low-noise device are shown in Figure 2-3a inset. After addition of 100 nM of protein sample, translocation signals were detected (Figure 2-3b).

Figure 2-3d-g shows the concatenated events of the MLP translocation through the nanopore with a Nutlin-3 concentration of 1:0, 1:1, 1:5, and 1:10. First, only single-peak events (type I) were observed in the samples without Nutlin-3 (Figure 2-3d). These results indicate that the MLP forms a single globular structure resulting from the interaction between p53TAD and MDM2. However, in the samples with a 1:1 molar ratio of Nutlin-3 and MLP (Figure 2-3e), a double-peak signal (type II) appeared as well as single-peak signals. More importantly, statistical information of the fraction of MLP and tMLP that is affected by Nutlin-3 can be obtained by counting the type II signals over the whole translocation signal. This way of

collecting statistical information is very different from other methods that rely on an ensemble approach. The fraction of type II events among all translocation events was 9.3 % (1:1), 12.0 % (1:5), and 23.0 % (1:10) as shown in Figure 2-3c.

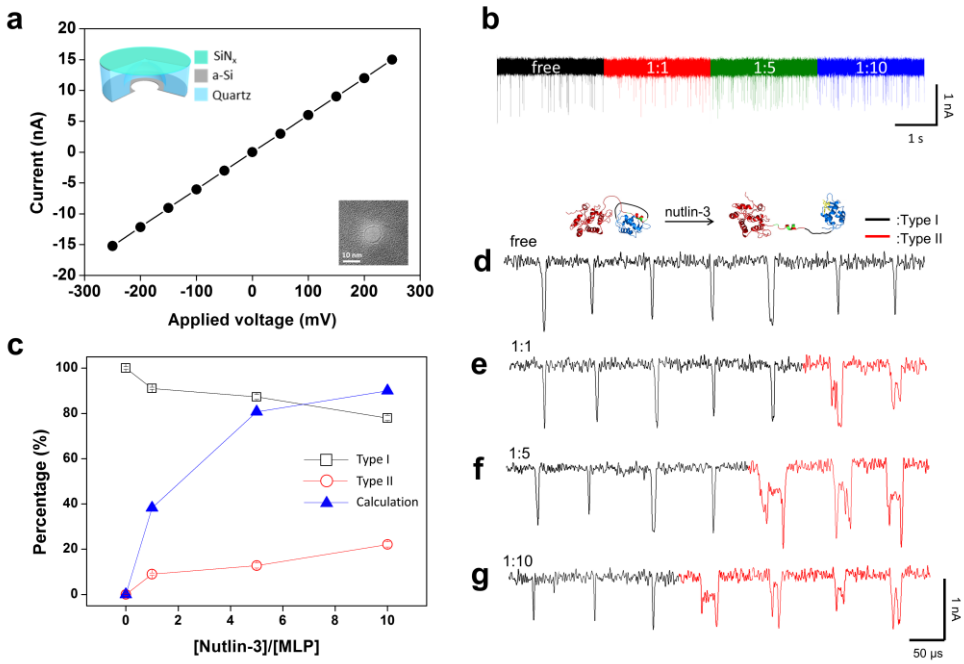

Figure 2-3. (a) I–V characteristic of the low-noise solid-state nanopore device. A schematic structure of the device and a transmission electron micrograph of the nanopore is shown in inset. (b) Continuous current trace of nanopore signal with respect to the molar ratio of Nutlin-3 to the MLP as free (black), 1:1 (red), 1:5 (green), and 1:10 (blue). (c) Percentage of detected type I and type II signals versus Nutlin-3 concentration. Concatenated events of the proteins for free (d), 1:1 (e), 1:5 (f), and 1:10 (g). Among single-peak type I signals (black), a distinctive finger print-like double peak is shown in type II events (red). Type II events were found only in the mixture of MLP and Nutlin-3. Data were acquired at 4.16 MHz sampling rate and low-pass filtered at 500 kHz.

To check the validity of the experimental results, we estimated the fraction of type I and type II events for each molar ratio of MLP and Nutlin-3 using calculation model for protein-ligand binding affinity from the dissociation equilibrium constant equation.[35] Employing the dissociation constant of p53TAD and MDM2 (K_{d} = ~600 nM) and that of Nutlin-3 and MDM2 (K_{d} = ~100 nM) reported in the literatures,[28-31] the estimated fraction of type II events for each molar ratio of MLP and Nutlin-3 was 38.2 % (1:1), 80.7 % (1:5), and 90.0 % (1:10), which shows higher than the one detected from nanopore (Figure 2-3c). One of the reason is that the sample is not property handled to guarantee all the possible interaction between Nutlin-3 and MDM2. For instance, for the Nutlin-3 to interact with MDM2, the original interaction between p53TAD and MDM2 should first be dissociated. This dissociation process may be a bottle-neck process for the full reaction between Nutlin-3 and MDM2. Another reason is that the linked structure of p53TAD and MDM2 may exhibit a lower K_{d} than the reported value owing spatial proximity between p53TAD and MDM2.[36, 37] Also, the different diffusivity of the proteins might lead to the protein molecule to approach the pore entrance in different rate. In the solid-state nanopore experiments, the biomolecules are driven through the nanopore by the applied electric field. Because most of the electrical field is applied near the entrance of the nanopore, the biomolecules should approach the pore entrance by the random motion, where the electrophoretic velocity overwhelms the diffusive velocity of the proteins, thereby electrophoretically driven through the

nanopore.[38] The conformational change of the protein can result in large differences in diffusivity. The estimated bulk diffusion coefficient (D_0) for MLP yields $D_{0,MLP}$ = 68.05 nm^2 μs^{-1}.[39] D_0 for tMLP was estimated to be lower than MLP ($D_{0,tMLP}$ = 45.40 nm^2 μs^{-1}), where tMLP is assumed to be a dumbbell.[40] This lower D_0 for tMLP might affect the translocation event frequency as explained above. Another possibility is that some type II signal events appeared as type I events owing to an insufficient time resolution of the detection system.

2.3.3. Current drop histogram of the translocation events

For further analysis of Nutlin-3 effect on nanopore signal, current drop histogram for free, 1:1, 1:5, and 1:10 are analyzed (Figure 2-4). In the sample without Nutlin-3, we obtained two distinct populations in the fractional current ($\Delta I/I_0$) histogram for type I signal. The mean fractional current ($<\Delta I/I_0>$) was extracted by fitting the Gaussian function as $<\Delta I/I_0>$ ~0.036 and ~0.070, respectively. The first population in the histogram accounts for bumping event, while the second population is regarded as single molecule translocation of MLP. Since current drop less than $\Delta I/I_0$ <0.035 exhibits dwell time of ~ 5 μs in the scatter plot (Figure 2-4, see text), we regarded those event as bumping event. After the addition of equimolar Nutlin-3, two populations were also appeared with similar fractional current drop to free, showing $<\Delta I/I_0>$ ~0.034 and ~0.071, respectively. The further increase of Nutlin-3 concentration on the MLP to 5 and 10-fold molar ratio of Nutlin-3 into the MLP shows $<\Delta I/I_0>$ ~0.077 and 0.068 for 1:5 and 1:10, respectively. The similar value of $<\Delta I/I_0>$ implies that Nutlin-3 does not change a net volume of protein but identical event for type I event in all concentration of Nutlin-3.

Obviously, no bumping event was detected in type II event for all Nutlin-3 concentration. As we designed, we found two intra-peaks in the type II event. As we designed, the intra-peaks reflect the volume of GST-p53TAD and MDM2. Because the volume of GST-p53TAD is larger than that of

MDM2, a larger peak is considered to the transient blockage of GST-p53TAD in the nanopore. Figure 2-4e-g shows the fractional current histogram of GST-p53TAD peak in the type II. On the other hand, the most of MLP volume is occupied GST-p53TAD, the mean fractional current of type II ($<\Delta I/I_0>$ ~0.073) is reflected similar value to the type I event.

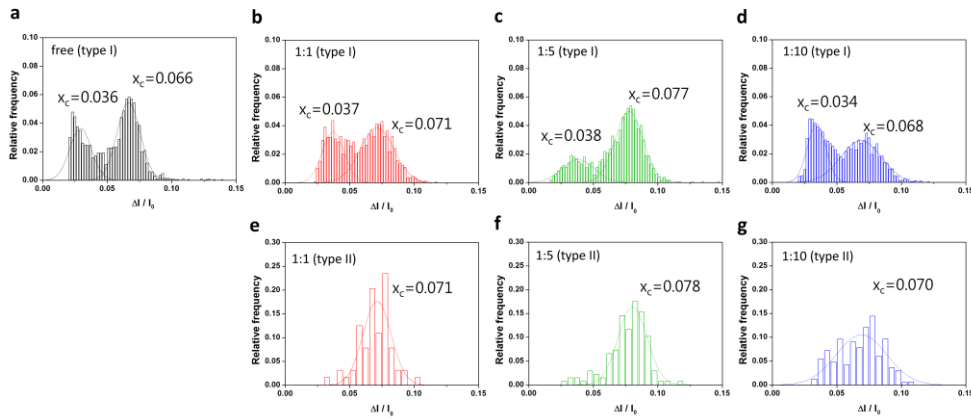

Figure 2-4. Scatter plot of fractional current drop versus dwell time for free (a), 1:1 (b), 1:5 (c), and 1:10 (d) molar ratios of MLP and Nutlin-3. Type II events (red star) were discriminated in type I events (black square) in the scatter plots. N~2000 events were collected for each Nutlin-3 concentration. Dwell time histogram of type I and type II events for free (e) 1:1 (f), 1:5 (g), and 1:10 (h). Only type I events are available for (a) and

2.3.4. Dwell time histogram of intra-peak of type II events

We additionally analyzed dwell time of type II event intra-peaks, which represents traversing time for GST-p53TAD, MDM2, and amino acid linker. Dwell time of type II intra-peak was defined as t_H, t_M, and t_L as shown in Figure 2-5a inset. Dwell time histogram for t_H was fitted by the Gaussian function with mean value, $<t_H>$, as 6.09±2.69, 5.85±5.44, and 5.70±3.18 μs for 1:1, 1:5, and 1:10, respectively. For $<t_M>$, we obtained lower value of 4.62±2.94, 5.40±4.91, and 4.59±3.09 μs for 1:1, 1:5, and 1:10, respectively. Data for t_L, which structurally reflects amino acid linker in our designed complex, exhibited short dwell time that fitting the Gaussian function to the data was not appropriated. We used the exponential decay function to evaluate the characteristic time for t_L yields 2.32, 2.44, and 2.15 μs for 1:1, 1:5, and 1:10, respectively.

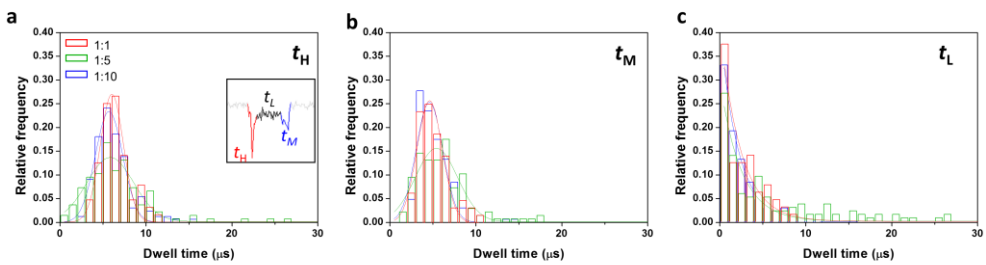

Figure 2-5. Histogram of dwell time for type II inter-event. Inset (a) represents the local dwell time of type II event (t_H, t_M and t_L). Dwell time histogram was fitted by the Gaussian function for t_H (a) and t_M (b), while dwell time histogram for t_L was fitted exponential decay function with characteristic time of 2.32, 2.44, and 2.15 μs for 1:1, 1:5, and 1:10, respectively.

2.3.5. Power spectrum density of the nanopore signal

To investigate the noise characteristics of the nanopore, the power spectrum density (PSD) of the nanopore signal measured at 0 mV and 200 mV are presented in Figure 2-6. The noise PSD was fitted to the polynomial form of $S = Af^{\beta} + B + Cf + Df^2$, where f is frequency in Hz and β is the fitting parameter ($0 < \beta < 2$)The parameters A, B, C, and D represent Flicker, Johnson (Nyquist), dielectric, and amplifier noise, respectively.[41] The corresponding fitting parameters are tabulated in Table 2-1.

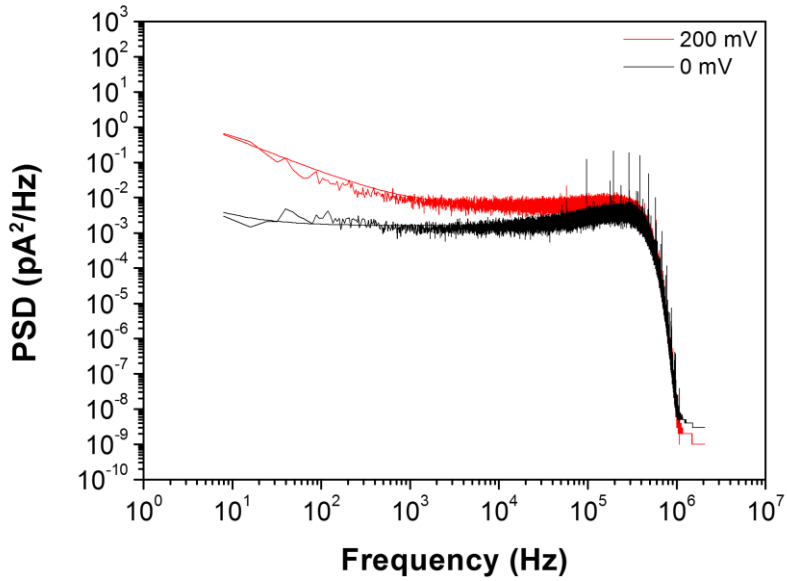

Figure 2-6. Power spectrum of silicon nitride nanopore signal with 1 M KCl in 1×PBS solution under 200 mV electric potential. Data was acquired using 4.16 MHz sampling rate and low-pass filtered at 500 kHz.

Table 2-1. Noise parameters of the nanopore device under 0 mV and 200 mV.

Noise parameters	**0 mV**	**200 mV**
A	1.77×10^{-2}	4.95
B	1.58×10^{-3}	5.89×10^{-3}
C	1.39×10^{-8}	5.19×10^{-9}
D	0	0
β	1	1
I_{rms} **(pA)**	38.76	51.76

2.3.6. Protein transport kinetics

Figure 2-7a-d shows the scatter plot of fractional current drop ($\Delta I/I_0$) *versus* dwell time for MLP with and without Nutlin-3 at different molar ratios of Nutlin-3 and MLP. While only type I event signals appeared in the samples without Nutlin-3 (Figure 2-7a), both type I (black squares) and II (red star) events appeared with the increasing molar ratios of Nutlin-3 and MLP (Figure 2-7b-d). These data clearly show that type II signals appeared in a longer dwell time range compared to type I signals.

Dwell time histograms were derived from the scatter plots and are presented in Figure 2-7e-f. The distribution of type II events in all Nutlin-3 concentrations clearly shows that tMLP exhibited a slower translocation through the pore. To quantitatively evaluate the translocation behavior of MLP and tMLP, we used the 1D diffusion-drift model proposed by Ling *et al.*;[42]

$$F(t) = \frac{h_{eff}}{\sqrt{4\pi D_p t^3}} e^{-\frac{(h_{eff} - v_d t)^2}{4 D_p t}} \quad (2)$$

where $F(t)$ is the probability density function, h_{eff} is the effective pore thickness, D_p is the protein diffusion coefficient inside the pore, and v_d is the drift velocity of the protein, respectively. We extracted the free parameters D_p and v_d for type I and II events by fitting the dwell time histograms to Eq. (2) ($R^2 > 0.96$). The obtained D_p for type I events were 4.92±0.10, 5.05±0.13,

4.57±0.10, and 5.19±0.09 $nm^2\ \mu s^{-1}$ for free, 1:1, 1:5, and 1:10, respectively. In contrast, the D_p values for type II events were much lower: 0.29±0.02, 0.33±0.01, and 0.37±0.02 $nm^2\ \mu s^{-1}$ for 1:1, 1:5, and 1:10, respectively. In addition, lower v_d values for type II events were acquired as 0.71±0.01, 0.66±0.01, and 0.79±0.01 nm μs^{-1} for 1:1, 1:5, and 1:10, respectively, whereas for type I events the values were 1.48±0.04, 1.46±0.02, and 1.44±0.04 nm μs^{-1}, respectively (1.46±0.02 nm μs^{-1} for free). The similar D_p and v_d values for each Nutlin-3 concentration reveals the identical structure of MLP and tMLP. On the other hand, lower D_p and v_d values were obtained for type II events, suggesting that the MLP structure changes into a slower and less diffusive state in the nanopore. Comparing the D_p values to the bulk diffusion coefficient shows that D_p for MLP was ~14 times smaller than D_0, indicating that the diffusive motion of MLP is severely retarded inside the nanopore. On the other hand, the D_p value for tMLP was ~137 smaller compared to $D_{0,tMLP}$, which is considered to reflect not only the spatial confinement in the nanopore but also a protein-pore interaction.[26, 38, 43, 44]

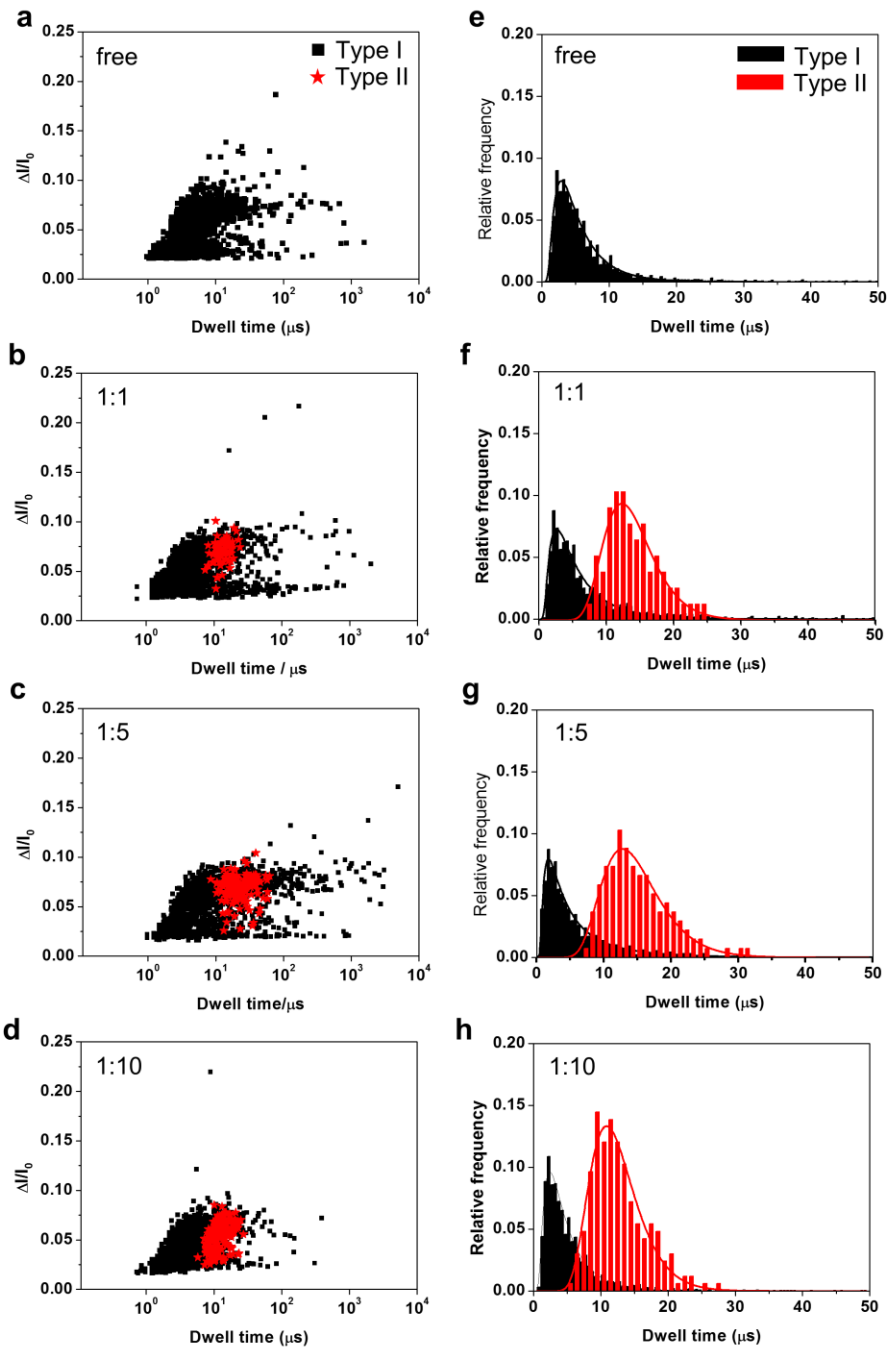

Figure 2-7. Scatter plot of fractional current drop versus dwell time for free (a), 1:1 (b), 1:5 (c), and 1:10 (d) molar ratios of MLP and Nutlin-3. Type II events (red star) were discriminated in type I events (black square) in the scatter plots. N~2000 events were collected for each Nutlin-3 concentration. Dwell time histogram of type I and type II events for free (e) 1:1 (f), 1:5 (g), and 1:10 (h). Only type I events are available for (a) and (e). Dwell time

histograms were fitted using eq. (2) (see text) for extracting free parameter of in-pore diffusion coefficient D_p and drift velocity v_d.

2.3.7. Voltage dependence of protein translocation

In order to investigate the voltage-dependent translocation of the proteins, additional nanopore experiment were performed as a function of applied voltage. We applied the electric potential of 100 mV, 150 mV, and 200 mV to protein mixture of 1:10 (MLP to Nutlin-3 ratio) and detected both type I and type II event translocation events as shown in Figure 2-8a. We analyzed dwell time histogram of both type I and type II event from the scatter plots (Figure 2-8b) and the 1D diffusion-drift function (Eq. (2)) was fitted to this data (R^2>0.93). From the fitted graph, the most probable value of dwell time of type II event was estimated as 16.00, 12.59, and 10.85 μs, for 100, 150, and 200 mV, respectively. The extracted drift velocity of both type I and type II event exhibit linear dependence to the applied voltage (Figure 2-8c). The mean electrophoretic mobility was estimated as 74.2±2.31 and 31.5±3.53 $nm^2ms^{-1}V^{-1}$ for type I and type II, respectively. The normalized capture rate (R_c/C_0; R_c is the measured capture rate, and C_0 is the bulk protein concentration, respectively) of type I and type II was shown in the Figure 2-8d. We observed that the normalized capture rate of type I event increases with a larger slope (0.20±0.01 $s^{-1}\,nM^{-1}\,mV^{-1}$) than that of type II (0.04±0.01 $s^{-1}\,nM^{-1}\,mV^{-1}$), but both type of event shows linear dependency to the applied voltage, reflecting that the protein captures were driven by electric field and limited by diffusion process.[45]

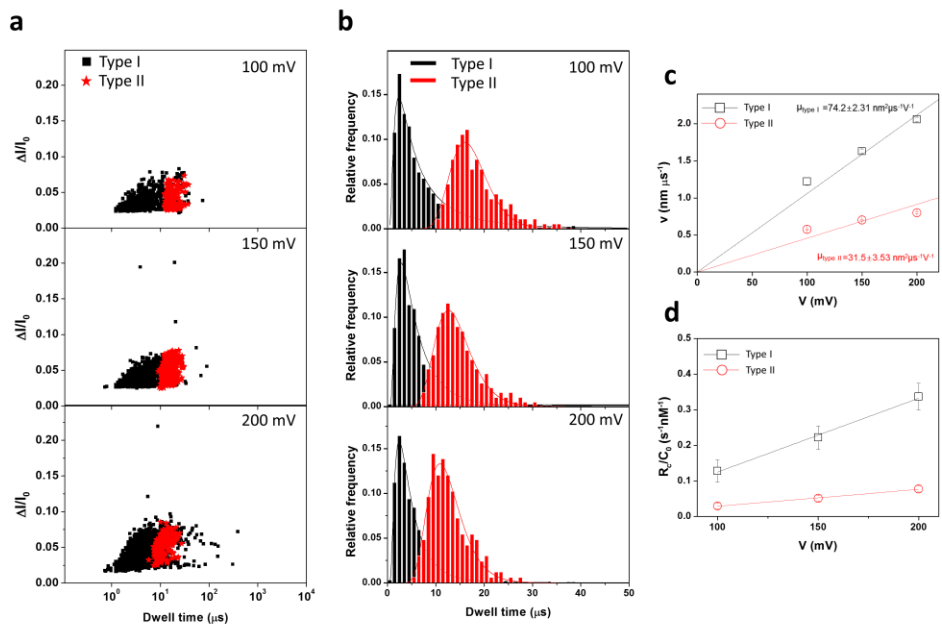

Figure 2-8. (a) Scatter plots of fractional current drop versus dwell time for type I and type II at the different voltages. (b) Dwell time distributions for type I and type II event varying electric potential. All histograms are fitted by 1D diffusion-drift model (see main text) ($R^2 > 0.95$). (c) Drift velocity of type I and type II event as a function of applied voltage. The drift velocity was extracted from the 1D diffusion-drift model and linearly increases to the increased applied voltage. (d) Normalized capture rate versus applied voltage.

2.3.8. Protein size analysis

Figure 2-9 shows histogram of fractional current for type II intra-peak. Since GST-p53TAD, MDM2, and amino acid linker exhibit different volume, three different current drop inside the type II event was measured. The intra-peak information of the signal was defined to I_H, I_M, and I_L for high-, mid-, and low-level of fractional current, respectively (Figure 2-9a inset). The mean fractional current, $<I_H>$, shows ~0.071, 0.077, and 0.068 for 1:1, 1:5, and 1:10, respectively. The $<I_M>$ value exhibits lower value to the $<I_H>$ showing $<I_M>$ ~0.044, 0.045, 0.044, for 1:1, 1:5, and 1:10, respectively. We found I_L, which structurally reflected by amino acid linker with mean value $<I_L>$ as 0.020, 0.019, and 0.022, for 1:1, 1:5, and 1:10, respectively. Each $<I_H>$, $<I_M>$ and $<I_L>$ values show consistent in all Nutlin-3 concentration condition, indicating identical signal. Since the structure of the protein complex used in the experiment can be divided into three parts, we assumed that the value I_H, I_M, and I_L represents each GST-p53TAD, MDM2, and amino acid linker, respectively. On the basis of the value, hydrodynamic diameter of the protein was estimated by using analytical solution[26, 38, 46]

$$d_m = [\left(\frac{\Delta I}{I_0}\right)\left(h_{eff} + 0.8d_p\right){d_p}^2]^{1/3} \quad (3)$$

where d_m is the protein diameter, h_{eff} is the effective thickness of the pore (7 nm), and d_p is the pore diameter (8 nm), respectively. The data yield d_m=

4.07±0.81, 3.49±1.10 nm for I_H and I_M, respectively. In comparison to the experimental results, x-ray crystallographic structure of GST-p53TAD and MDM2 were referred from Protein Data Bank (PDB code: 1BG5; GST-p53TAD, 1YCR; MDM2). The estimated physical dimension of crystallographic structure for GST-p53TAD and MDM2 yields 4.7×5.3×6.0 and 2.4×2.6×4.1 nm^3, respectively. Considering the crystallized protein sample in x-ray diffraction measurement undergoes quite different surrounding environment to the aqueous solution, our nanopore result well reflects the different size of the proteins.

Whereas GST-p53TAD and MDM2 are assumed as globular structures, we assumed that the amino acid linker exhibits cylindrical structures. By taking the amino acids linker as membrane-thick long cylinder, the estimated diameter of the cylinder yields 2.72±1.47 nm. This result is ~5 times larger than the reported results.[47] It is not clearly known but probably the linker is not fully stretched when passing through the nanopore. It is also possible that due to fast translocation speed, the I_L, which is located in-between GST-p53TAD and MDM2 intra-peaks, was not sufficiently resolved.

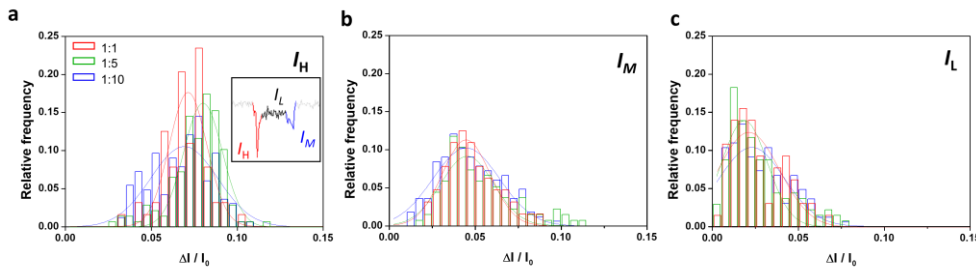

Figure 2-9. Fractional current drop histogram of type II intra-event. Fractional current drop histogram of I_H (a), I_M (b), and I_L (c) of type II event. Inset (a) represents the local fractional current drop of type II event (I_H, I_L and I_M). Fractional current drop histogram of local peak parameters for 1-fold (red), 5-fold (green) and 10-fold Nutlin-3 added MLP (blue). All histograms were fitted by the Gaussian function.

2.4. Summary and conclusions

In this chapter, we have demonstrated the detection of Nutlin-3-induced conformational change in the MLP using solid-state nanopores. The characteristic double-peak was successfully detected using a high-frequency amplifier (4.16 MHz), combined with our low-noise solid-state nanopore device. Increased concentration of Nutlin-3 resulted in an increased appearance of double-peaks. The in-pore diffusion coefficient determined for MLP by applying the 1D diffusion-drift model was ~14 times smaller than the bulk diffusion coefficient, and ~137 times smaller than that observed for tMLP. Our nanopore experiments suggest that drug-induced conformational changes in proteins can be monitored at the single molecule level and our system enables the efficient prediction of drug effects on a protein complex. Moreover, the analyzed local signal of type II intra-peak probed the conformation and size of our designed protein complex. These results indicate a potential application of solid-state nanopore sensors in drug screening against diverse PPI targets and in protein conformational studies.

2.5. References

1. Chae, H.; Kwak, D.-K.; Lee, M.-K.; Chi, S.-W.; Kim, K.-B. J. N., Solid-state nanopore analysis on conformation change of p53TAD–MDM2 fusion protein induced by protein–protein interaction. **2018,** *10* (36), 17227-17235.

2. Wells, J. A.; McClendon, C. L., Reaching for high-hanging fruit in drug discovery at protein–protein interfaces. *Nature* **2007,** *450* (7172), 1001.

3. Campillos, M.; Kuhn, M.; Gavin, A.-C.; Jensen, L. J.; Bork, P., Drug target identification using side-effect similarity. *Science* **2008,** *321* (5886), 263-266.

4. Arkin, M. R.; Wells, J. A., Small-molecule inhibitors of protein–protein interactions: progressing towards the dream. *Nature reviews Drug discovery* **2004,** *3* (4), 301.

5. Nero, T. L.; Morton, C. J.; Holien, J. K.; Wielens, J.; Parker, M. W., Oncogenic protein interfaces: small molecules, big challenges. *Nature Reviews Cancer* **2014,** *14* (4), 248.

6. Mittermaier, A.; Meneses, E., Analyzing Protein–Ligand Interactions by Dynamic NMR Spectroscopy. In *Protein-Ligand Interactions*, Springer: 2013; pp 243-266.

7. Perumal, V.; Hashim, U., Advances in biosensors: Principle, architecture and applications. *Journal of Applied Biomedicine* **2014,** *12* (1), 1-15.

8. Janzen, W. P., Screening technologies for small molecule discovery: the state of the art. *Chemistry & biology* **2014,** *21* (9), 1162-1170.

9. Seo, Y.; Jeong, S.; Lee, J.; Choi, H. S.; Kim, J.; Lee, H., Innovations in biomedical nanoengineering: nanowell array biosensor. *Nano Convergence* **2018,** *5* (1), 9.

10. El-Said, W. A.; Yoon, J.; Choi, J.-W., Nanostructured surfaces for analysis of anticancer drug and cell diagnosis based on electrochemical and SERS tools. *Nano Convergence* **2018,** *5* (1), 11.

11. Homola, J.; Yee, S. S.; Myszka, D., Chapter 4 - SURFACE PLASMON RESONANCE BIOSENSORS. In *Optical Biosensors (Second Edition)*, Elsevier: Amsterdam, 2008; pp 185-242.

12. Shi, X.; Gao, R.; Ying, Y.-L.; Si, W.; Chen, Y.-F.; Long, Y.-T., A Scattering Nanopore for Single Nanoentity Sensing. *ACS Sensors* **2016,** *1* (9), 1086-1090.

13. Sha, J.; Shi, H.; Zhang, Y.; Chen, C.; Liu, L.; Chen, Y., Salt Gradient Improving Signal-to-Noise Ratio in Solid-State Nanopore. *ACS sensors* **2017,** *2* (4), 506-512.

14. Uram, J. D.; Ke, K.; Hunt, A. J.; Mayer, M., Submicrometer Pore-Based Characterization and Quantification of Antibody–Virus Interactions. *Small* **2006,** *2* (8-9), 967-972.

15. Uram, J. D.; Ke, K.; Hunt, A. J.; Mayer, M., Label-Free Affinity Assays by Rapid Detection of Immune Complexes in Submicrometer Pores. *Angewandte Chemie International Edition* **2006,** *45* (14), 2281-2285.

16. Han, A.; Creus, M.; Schürmann, G.; Linder, V.; Ward, T. R.; de Rooij, N. F.; Staufer, U., Label-free detection of single protein molecules and protein− protein interactions using synthetic nanopores. *Analytical chemistry* **2008,** *80* (12), 4651-4658.

17. Wei, R.; Gatterdam, V.; Wieneke, R.; Tampé, R.; Rant, U., Stochastic sensing of proteins with receptor-modified solid-state nanopores. *Nature nanotechnology* **2012,** *7* (4), 257-263.

18. Lin, Y.; Ying, Y.-L.; Shi, X.; Liu, S.-C.; Long, Y.-T., Direct sensing of cancer biomarkers in clinical samples with a designed nanopore. *Chemical Communications* **2017,** *53* (84), 11564-11567.

19. Oukhaled, A.; Cressiot, B.; Bacri, L.; Pastoriza-Gallego, M.; Betton, J.-M.; Bourhis, E.; Jede, R.; Gierak, J.; Auvray, L. c.; Pelta, J., Dynamics of completely unfolded and native proteins through solid-state nanopores as a function of electric driving force. *ACS nano* **2011,** *5* (5), 3628-3638.

20. Talaga, D. S.; Li, J., Single-molecule protein unfolding in solid state nanopores. *Journal of the American Chemical Society* **2009,** *131* (26), 9287-9297.

21. Madampage, C. A.; Tavassoly, O.; Christensen, C.; Kumari, M.; Lee, J. S., Nanopore analysis: An emerging technique for studying the folding and misfolding of proteins. *Prion* **2012,** *6* (2), 116-123.

22. Lin, Y.; Shi, X.; Liu, S.-C.; Ying, Y.-L.; Li, Q.; Gao, R.; Fathi, F.; Long, Y.-T.; Tian, H., Characterization of DNA duplex unzipping

through a sub-2 nm solid-state nanopore. *Chemical Communications* **2017,** *53* (25), 3539-3542.

23. Wang, H.-Y.; Ying, Y.-L.; Li, Y.; Kraatz, H.-B.; Long, Y.-T., Nanopore analysis of β-amyloid peptide aggregation transition induced by small molecules. *Analytical chemistry* **2011,** *83* (5), 1746-1752.

24. Freedman, K. J.; Bastian, A. R.; Chaiken, I.; Kim, M. J., Solid-State Nanopore Detection of Protein Complexes: Applications in Healthcare and Protein Kinetics. *Small* **2013,** *9* (5), 750-759.

25. Yusko, E. C.; Prangkio, P.; Sept, D.; Rollings, R. C.; Li, J.; Mayer, M., Single-particle characterization of Aβ oligomers in solution. *ACS nano* **2012,** *6* (7), 5909-5919.

26. Waduge, P.; Hu, R.; Bandrakar, P.; Yamazaki, H.; Cressiot, B.; Zhao, Q.; Whitford, P.; Wanunu, M., Nanopore-Based Measurements of Protein Size, Fluctuations, and Conformational Changes. *ACS nano* **2017**.

27. Kwak, D. K.; Chae, H.; Lee, M. K.; Ha, J. H.; Goyal, G.; Kim, M. J.; Kim, K. B.; Chi, S. W., Probing the Small-Molecule Inhibition of an Anticancer Therapeutic Protein-Protein Interaction Using a Solid-State Nanopore. *Angewandte Chemie International Edition* **2016,** *55* (19), 5713-5717.

28. Kussie, P. H.; Gorina, S.; Marechal, V.; Elenbaas, B.; Moreau, J.; Levine, A. J.; Pavletich, N. P., Structure of the MDM2 oncoprotein bound to the p53 tumor suppressor transactivation domain. *Science* **1996,** *274* (5289), 948-953.

29. Schon, O.; Friedler, A.; Bycroft, M.; Freund, S. M.; Fersht, A. R., Molecular mechanism of the interaction between MDM2 and p53. *Journal of molecular biology* **2002,** *323* (3), 491-501.

30. Fesik, S. W., Promoting apoptosis as a strategy for cancer drug discovery. *Nature Reviews Cancer* **2005,** *5* (11), 876.

31. Vassilev, L. T.; Vu, B. T.; Graves, B.; Carvajal, D.; Podlaski, F.; Filipovic, Z.; Kong, N.; Kammlott, U.; Lukacs, C.; Klein, C., In vivo activation of the p53 pathway by small-molecule antagonists of MDM2. *Science* **2004,** *303* (5659), 844-848.

32. Delaglio, F.; Grzesiek, S.; Vuister, G. W.; Zhu, G.; Pfeifer, J.; Bax, A., NMRPipe: a multidimensional spectral processing system based on UNIX pipes. *Journal of biomolecular NMR* **1995,** *6* (3), 277-293.

33. Lee, M.-H.; Kumar, A.; Park, K.-B.; Cho, S.-Y.; Kim, H.-M.; Lim, M.-C.; Kim, Y.-R.; Kim, K.-B., A low-noise solid-state nanopore platform based on a highly insulating substrate. *Scientific reports* **2014,** *4*, 7448.

34. Ha, J.-H.; Shin, J.-S.; Yoon, M.-K.; Lee, M.-S.; He, F.; Bae, K.-H.; Yoon, H. S.; Lee, C.-K.; Park, S. G.; Muto, Y., Dual-site interactions of p53 protein transactivation domain with anti-apoptotic Bcl-2 family proteins reveal a highly convergent mechanism of divergent p53 pathways. *Journal of Biological Chemistry* **2013,** *288* (10), 7387-7398.

35. Shortridge, M. D.; Hage, D. S.; Harbison, G. S.; Powers, R., Estimating protein− ligand binding affinity using high-throughput screening

by NMR. *Journal of combinatorial chemistry* **2008,** *10* (6), 948-958.

36. Krishnamurthy, V. M.; Semetey, V.; Bracher, P. J.; Shen, N.; Whitesides, G. M., Dependence of effective molarity on linker length for an intramolecular protein− ligand system. *Journal of the American Chemical Society* **2007,** *129* (5), 1312-1320.

37. Nagamune, T., Biomolecular engineering for nanobio/bionanotechnology. *Nano Convergence* **2017,** *4* (1), 9.

38. Larkin, J.; Henley, R. Y.; Muthukumar, M.; Rosenstein, J. K.; Wanunu, M., High-bandwidth protein analysis using solid-state nanopores. *Biophysical journal* **2014,** *106* (3), 696-704.

39. Young, M.; Carroad, P.; Bell, R., Estimation of diffusion coefficients of proteins. *Biotechnology and Bioengineering* **1980,** *22* (5), 947-955.

40. La Torre, D.; Garcia, J.; Bloomfield, V. A., Hydrodynamic properties of macromolecular complexes. I. Translation. *Biopolymers* **1977,** *16* (8), 1747-1763.

41. Dimitrov, V.; Mirsaidov, U.; Wang, D.; Sorsch, T.; Mansfield, W.; Miner, J.; Klemens, F.; Cirelli, R.; Yemenicioglu, S.; Timp, G., Nanopores in solid-state membranes engineered for single molecule detection. *Nanotechnology* **2010,** *21* (6), 065502.

42. Ling, D. Y.; Ling, X. S., On the distribution of DNA translocation times in solid-state nanopores: an analysis using Schrödinger's first-passage-time theory. *Journal of Physics: Condensed Matter* **2013,** *25* (37),

375102.

43. Niedzwiecki, D. J.; Grazul, J.; Movileanu, L., Single-molecule observation of protein adsorption onto an inorganic surface. *Journal of the American Chemical Society* **2010,** *132* (31), 10816-10822.

44. Cressiot, B.; Oukhaled, A.; Patriarche, G.; Pastoriza-Gallego, M.; Betton, J.-M.; Auvray, L. c.; Muthukumar, M.; Bacri, L.; Pelta, J., Protein transport through a narrow solid-state nanopore at high voltage: experiments and theory. *ACS nano* **2012,** *6* (7), 6236-6243.

45. Wanunu, M.; Morrison, W.; Rabin, Y.; Grosberg, A. Y.; Meller, A., Electrostatic focusing of unlabelled DNA into nanoscale pores using a salt gradient. *Nature Nanotechnology* **2009,** *5*, 160.

46. DeBlois, R.; Bean, C., Counting and sizing of submicron particles by the resistive pulse technique. *Review of Scientific Instruments* **1970,** *41* (7), 909-916.

47. Counterman, A. E.; Clemmer, D. E., Volumes of individual amino acid residues in gas-phase peptide ions. *Journal of the American Chemical Society* **1999,** *121* (16), 4031-4039.

Chapter 3. Statistical Analysis of the Binding Affinity of Small Molecules to MDM2 Protein Using Solid-State Nanopores

3.1. Introduction

While there are remarkable accomplishments in nucleic acids, only a few results have been reported for titration of drug into protein complex or protein-protein interactions. Protein-protein interactions (PPIs) are involved in metabolisms, cell signaling, and gene regulatory networks. Thus mediating PPI by drug molecule is key target for molecular studies for human diseases.[1] Also, due to extremely high specificity of the interaction, PPIs are highlighted as an attractive drug screening target.[2] While nucleic acids exhibit linear conformation with uniformly charged structure, proteins have variety of structures with heterogeneous charge distribution. Since protein has three-dimentional structure, the orientation varies during translocation, which might cause inconsistent current drop. Since estimating binding affinity by current drop change is limited to the molecules that i) measured in consistent current drop for drug-free state, and ii) cause a volume expansion upon ligand binding, the quantitative evaluation of dissociation equilibrium in protein-small-ligand interface is challenging.

In order to investigate protein-protein interaction and its inhibition by small ligand, we have discussed in the chapter 1.3.2 with a new approach proposed by Kwak *et al*, probed the interaction of glutathione-S-transferase tagged cancer target protein of p53 transactivation domain (GST-p53TAD) and MDM2 and its inhibition by monitoring change in event frequency of MDM2.[3] Upon binding of GST-p53TAD with MDM2, the net charge of positively charged MDM2 is inversed due to the charge masking by

negatively charged GST-p53TAD. The addition of Nutlin-3, which known as a small-molecule MDM2 antagonist, inhibits GST-p53TAD-MDM2 interaction and liberates MDM2 from the complex. Thus, the restoration of the event frequency of MDM2 was successfully measured. However, this approach is not generally applicable since there are plentiful protein-protein or protein-ligand interactions without changing the net charge.

Advanced from monitoring event frequencies, the recent study as discussed in the chapter 2, which demonstrated the inhibition of p53TAD-MDM2 interaction by monitoring drug-induced conformational change of the protein.[4] In order to induce conformational change, we connected GST-p53TAD and MDM2 by amino acid linker (MLP). Since the binding affinity of Nutlin-3 and MDM2 is higher than p53 and MDM2[5-7], the direct interaction of Nutlin-3 and MDM2 releases the GST-p53TAD domain from MLP, thereby transforms its conformation from globular to dumbbell shape (tMLP) as Nutlin-3 addition. As expected, translocation signal of globular-shaped protein exhibits single-peak signal (type I), whereas dumbbell-shaped protein shows double-peak signal (type II) due to its relatively larger volume at each terminal. By counting type II event among whole translocation event the binding fraction of Nutlin-3 ($f_{\text{Nutlin-3}}$) was calculated, yielding increased $f_{\text{Nutlin-3}}$ value from 9.3% to 23.0% as the molar ratio of Nutlin-3 to MLP is increased from 1:1 to 1:10, respectively. This approach is a novel method for identifying PPI and its inhibition by small-molecule, but the further quantitative estimation of binding affinity was not attainable

owing to unclarified resolution limit of the type II event in our measurement system (sampling rate: 4.16 MHz). In this chapter, we discuss the demonstrated result of nanopore titration for four small-molecules into MLP protein complex, by revealing the detection limit of all dumbbell-shaped protein.

3.2. Experimental details

Nanopore experiment

Low-noise quartz-based solid-state nanopore device was fabricated as described by the previous report.[8] Before measurement, the nanopore device was cleaned by the mixture of sulfuric acid (H_2SO_4) and hydrogen peroxide (H_2O_2) solution in 3 to 1 ratio. After then, the nanopore device is assembled between PDMS gasket with the custom made Teflon flow cell. Next, the flow cell is placed in a Faraday cage after filling 1 M KCl in 1×PBS buffer (pH=7.4) in the *cis* and *trans* chambers. In all protein experiment, the concentration of mMLP or MLP is fixed into 100 nM and was introduced only in the *cis* chamber. For the titration experiments, the inhibitor was induced in 100 nM of MLP solution and incubated for 2 hours in room temperature. Each mixture with different inhibitor molar ratio is prepared and measured separately. The translocation events were recorded under 200 mV potential across the membrane using Ag/AgCl electrode. Data were collected using Chimera VC 100 (Chimera Instruments, USA) with sampling rate of 4.16 MHz and 500 kHz low-pass filter is applied. The data was converted into binary file by using python 2.7 based program “pythion” (Developed in Wanunu group) and analyzed by Clampfit 10.4 (Molecular Devices, CA, USA) and described using OriginPro 8 (OriginLab, MA, USA) software.

Expression and purification of proteins (Courtesy of KRIBB)[⑤]

The MLP protein (MDM2 (residues 3-109)-linker-p53TAD (1-73)-GST) and mutant MLP protein (substitution of 15-29 resdiues of p53TAD to $(GGGS)_3GGS$ residues in MLP) were expressed in *Escherchia coli* Rosetta™2 cells by induction with 0.5 mM isopropyl-β-D-thiogalactoside (IPTG) at an OD_{600} of 0.7. After cell culture for 16 hours at 20 ℃ and then the cells were harvested for the purification. The MLP protein was purified by GST affinity chromatography (GSTrap™, GE healthcare), anion exchange chromatography (Hitrap™ Q, GE healthcare), and size-exclusion chromatography (HiLoad® 16/600 Superdex® 75 pg, GE healthcare), as previously described.[8]

[⑤] Dr. Seung-Wook Chi and Dong-Kyu Kwak in Korea Research Institute of Bioscience and Bioengineering (KRIBB) (swchi@kribb.re.kr, dikay@kribb.re.kr)

Isothermal Titration Calorimetry (ITC) (Courtesy of KRIBB)[⑥]

The ITC measurements were performed at 25 ℃ in the reaction buffer containing 1 × PBS (pH 7.4) using an Auto-iTC$_{200}$ calorimeter (GE healthcare) in the Korea Basic Science Institute. Nutlin-3 (Cayman Chemical Inc.), NSC66811 (Tocris Bioscience), and SC204072 (SantaCruz) were commercially purchased and then dissolved in 100 % DMSO for 4 mM stock solutions. The final concentration of DMSO used for each ITC measurement was lower than 5 % (v/v). Titration experiment was carried out by 19 injections (2.0 μL per injection) of each inhibitor into the 5 μM MLP protein solution. The ITC data were analyzed using Origin™ software (MicroCal). All K_d values were determined through the global fitting using one-set-of-site model.

⑥ Dr. Seung-Wook Chi and Dong-Kyu Kwak in Korea Research Institute of Bioscience and Bioengineering (KRIBB) (swchi@kribb.re.kr, dikay@kribb.re.kr)

3.3. Results and discussion

Figure 3-1a depicts the translocation of the globular shaped MLP and the dumbbell shaped tMLP through low-noise ~10 nm thick silicon nitride (SiN) nanopore[9] with a diameter of d ~ 8 nm (micrograph shown in Figure 3-1a inset). The expected nanopore signal of MLP with (i) and without drug treatment (ii) is distinguished as single-peak of type I and the characteristic double-peak of type II event, respectively. Our nanopore measurement concept is illustrated in Figure 3-1b, showing the estimation of the K_d value by measuring the type II event fraction of the nanopore signal from the different drug molecules.

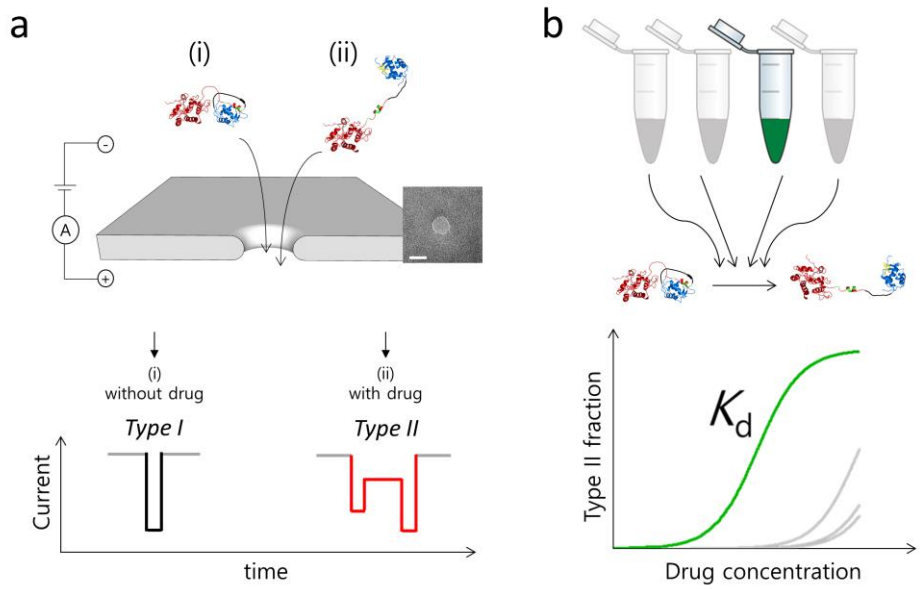

Figure 3-1. Illustration of nanopore titration. (a) Nanopore detection of the globular shaped MLP (i) and the drug-bound dumbbell shaped tMLP (ii). The expected peak signal of MLP with and without drug molecule addition. A single-peak signal of MLP molecule translocation and a characteristic double-peak signal of tMLP are schematically depicted. Nanopores with a diameter of ~8 nm were drilled by focused electron beam and the representative electron micrograph of is shown in the inset (scale bar is 10 nm). (b) A conceptual sketch of estimating K_d value of inhibitors from the type II event fraction.

3.3.1. Resolution of nanopore measurement for double-peak signal detection

In order to reveal the resolution of our measurement system for discriminating the double-peak signal, we introduced a modified MLP protein complex (mutant MLP; mMLP) by replacing a 15 residues of p53TAD (residues 15-29) with an amino acid residue $(GGGS)_3GGS$ to form a dumbbell shape without any drug treatment. Since p53TAD of mMLP has no binding motif toward MDM2, mMLP structure exhibits all-dumbbell-shaped conformation in solution. The translocation events of mMLP were measured at electric potential of 200 mV by varying cutoff frequency (f_c) to the identical data. Figure 3-2a shows the scatter plots of normalized current drop $\Delta I/I_0$ *versus* dwell time of mMLP translocation events, where ΔI is current drop and I_o is open-pore current, respectively. We applied low-pass filter ranging f_c = 100 - 1000 kHz to the recorded data, revealed that the double-peak signal of mMLP could not be resolved less than f_c < 500 kHz due to a severe distortion of the data (Figure 3-2a inset). This result implies that the dumbbell-shaped mMLP could be detected as a type I event, even a passing molecule whose actual structure is a dumbbell. We note that the type I event is still appeared even at f_c >500 kHz, suggesting the resolution limit for discriminating the type II event in the measurement system. It is considered that the amino acid linker in mMLP might present in a folded form in solution, which reduces the distance between two spherical domains,

thereby insufficient length to distinguish signals of the domains in the measurement system. The type I events might also be appeared in the translocation signals of all-dumbbell-shaped mMLP due to the fast translocation speed of the protein molecules, which might cause a data distortion under the insufficient filter bandwidth.[10] We observed the maximum type II fraction, f_{mMLP}, at f_c = 500 kHz, showing f_{mMLP}= 0.84 and slightly decreased to 0.69 at f_c = 1 MHz (Figure 3-2b). Figure 3-2c displays a normalized capture rate (R_c/C_0; where R_c is capture rate, and C_0 is protein concentration, respectively) as a function of cutoff frequency, showing an increased R_c/C_0 with increasing f_c and saturated at 500 kHz. We considered that an undetected translocation event with distorted ΔI amplitude less than I_o fluctuation at deficient f_c becomes detectable as f_c is increased; however, we observed the saturated R_c/C_0 at f_c = 500 kHz (0.47 s^{-1} nM^{-1} for type I and 0.15 s^{-1} nM^{-1} for type II, respectively), implying that the measurement condition of f_c coupled with our low-noise device resolves the undetected event but further resolving is still limited by significant electric noise generated by the high-frequency amplifier.

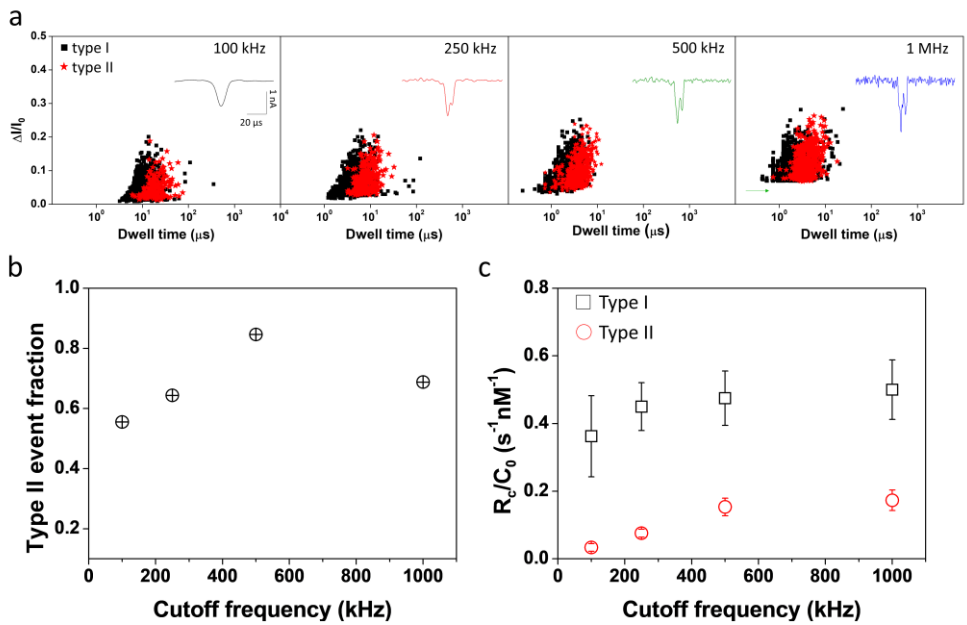

Figure 3-2. Discriminating type I and type II events through nanopore signal of mMLP molecule. (a) Scatter plots of $\Delta I/I_0$ *versus* dwell time for type I and type II events low-pass filtered at the indicated frequency (N ~ 2,000 events). Distortion of a representative type II event filtered to the one identical data (inset). Green arrow represents the current fluctuation of base line upon increased cutoff frequency. (b) Type II event fraction as function of cutoff frequency. The maximum type II fraction was found at f_c = 500 kHz. (c) Normalized capture rate.

3.3.2. Comparison of intra-molecular structure of tMLP and mMLP

To discover that the structural change of MLP is caused by the binding of Nutlin-3, we compared the type II event appeared in tMLP and mMLP. Since the inhibition of interaction between GST-p53TAD and MDM2 leads to the structural change, the structure of tMLP and mMLP is expected to be identical. To detect translocation signal of tMLP, we applied 15-fold molar ratio of Nutlin-3 to the MLP and measured under the experimental condition at f_c = 500 kHz, where the maximum resolution of double-peak was discriminated in the mMLP experiment. Figure 3-3a presents the scatter plot of $\Delta I/I_0$ *versus* dwell time of the translocation events of MLP with 15-fold molar ratio of Nutlin-3. Unlike MLP with absence of Nutlin-3, the characteristic double peak signal from tMLP is newly appeared by addition of Nutlin-3 (Figure 3-3a inset). Compared to the tMLP, the scatter plot of mMLP shows consistent in data distribution of type II event (Figure 3-3b). To quantitatively investigate the type II event observed in tMLP and mMLP, the intra-peak of each type II event was analyzed. Since the volume difference of GST-p53TAD, MDM2, and amino acid linker is reflected by current drop amplitude in the type II signal, each current drop is defined as I_P, I_M, and I_L, respectively. Figure 3-3c-e show the histogram of the fractional current drop of the intra-peaks. The Gaussian function was fitted to the data, yielding the mean fractional current drop of the best fit to tMLP

data as 0.072, 0.045, and 0.022 for I_P, I_M, and I_L, respectively. For mMLP, the mean fractional current drop of I_P, I_M, and I_L shows 0.073, 0.046, and 0.021, respectively. These values are in consistent, supporting that the type II event in tMLP and mMLP are reflected by the identical molecular structure.

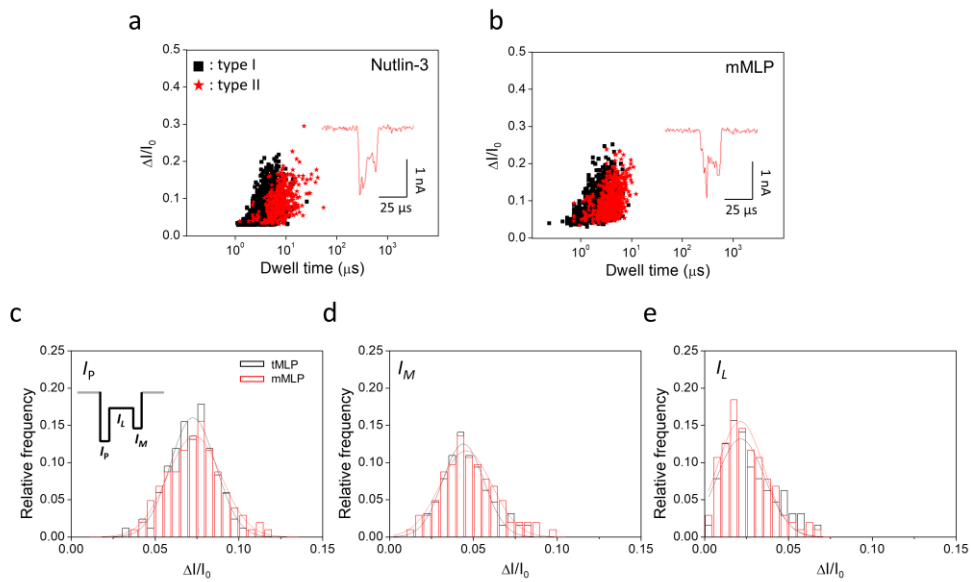

Figure 3-3. Comparison of the intra-molecular structure of tMLP and mMLP. Scatter plot of normalized current drop *versus* dwell time for MLP with 15-fold Nulin-3 (a) and mMLP translocation event (b). Type I (black square) and type II events (red star) are discriminated in the scatter plots. The representative type II signal is presented in the inset. (c-e) Histogram of normalized current drop of the intra-peak in the type II signal of tMLP (black) and mMLP (red). I_P, I_M, and I_L represent the normalized current drop of GST-p53TAD (I_P), MDM2 (I_M), and amino acid linker (I_L) part in the tMLP and mMLP, respectively. All histograms are fitted by the Gaussian function ($R^2 > 0.92$).

3.3.3. Evaluation of binding affinity of p53TAD/MDM2 interaction inhibitors by measuring type II event fraction

Since the binding of the drug molecule to MLP leads to the appearance of type II event, we demonstrated the evaluation of the binding affinity of potential inhibitors of GST-p53TAD/MDM2 interaction (Nutlin-3, NSC66811, and SC204072) by measuring type II event fraction. Figure 3-4a presents molecular structure of the inhibitors and MMC was examined as a negative control. The type II event fraction was measured by increasing molar concentration of inhibitors into MLP protein. Since we found the detection limit of the type II event from the mMLP translocation experiment results, we applied low-pass filter at f_c = 500 kHz in titration experiments, where the maximum type II event fraction could be resolved in our measurement system. Thus, the measured type II fraction in the titration result was calibrated by dividing f_{mMLP}. Figure 3-4b shows the calibrated type II event fraction as a function of the molar ratio of the inhibitors to the MLP. We observed the increased type II event fraction as increased molar ratio of the inhibitors. To quantitatively evaluate the drug effect on MLP, the simple binding model (eq. (1)) was fitted to the data (R^2>0.96), yielding the free parameter of K_d as 0.59±0.04 μM, 0.81±0.01 μM, and 2.65±18 μM for Nutlin-3, NSC66811, and SC204072, respectively. Unlike the potential inhibitors, the negative control of MMC shows no increase in type II event fraction with increasing concentration, suggesting that MMC is a chemical

that does not bind to MDM2 and thus, type II events are signals that occur only when the interaction between GST-p53TAD and MDM2 is inhibited.

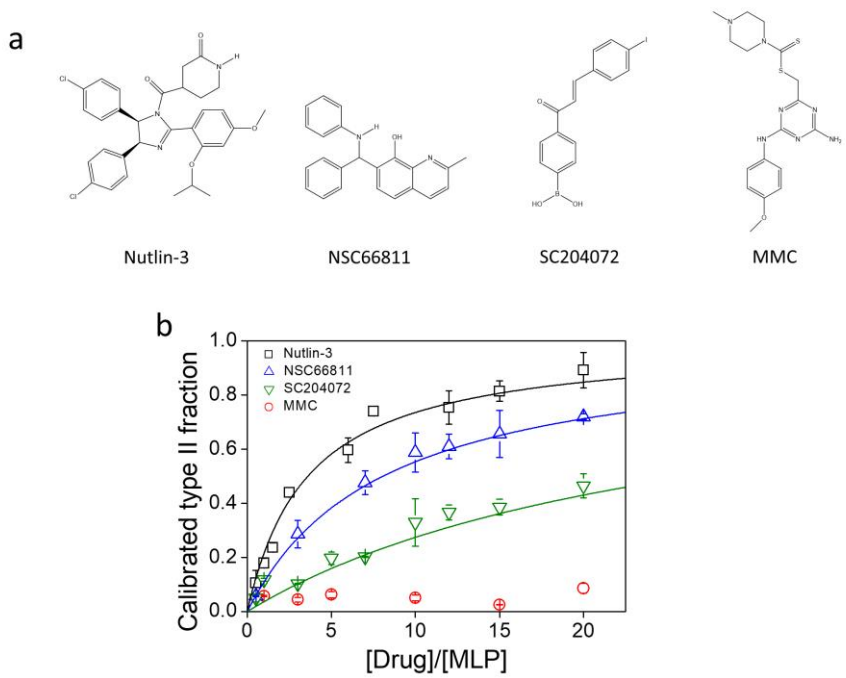

Figure 3-4. Nanopore titration of potential inhibitor of the interaction between p53 and MDM2. (a) Chemical structure of inhibitrs (Nutlin-3, NSC66811, and SC204072). ((4-amino-6-((4-methoxyphenyl)amino)-1,3,5-triazin-2-yl)methyl 4-methylpiperazine-1-carbodithioate (MMC) is introduced as a negative control. (b) Calibrated type II fraction *versus* molar ratio of drug to MLP along with the fits to the binding model (eq. 1) with K_d as a free parameter.

3.3.4. Isothermal titration calorimetry (ITC) experiment

To confirm the binding affinity of PPI inhibitors to MLP, Dr. Seung-Wook Chi and Dong-Kyu Kwak measured K_d for three PPI inhibitors using isothermal titration calorimetry (ITC). The ITC experiment was performed by the titration of each inhibitor (50-75 μM) to 5 μM of MLP sample (Figure 3-5). As shown in Table 3-1, the determined K_d values of Nutlin-3, NSC66811, and SC204072 are 0.79±0.19 μM, 0.95±0.17 μM, and 1.72±0.39 μM, respectively. Although K_d values obtained from the nanopore-based detection are not precisely matched to those of ITC measurements, the order of binding affinity (Nutlin-3 < NSC66811 < SC204072) is consistent between ITC and nanopore results. Finally, our data suggests that nanopore-based monitoring of conformational changes of MLP can be a valuable approach to determination of K_d for PPI inhibitors.

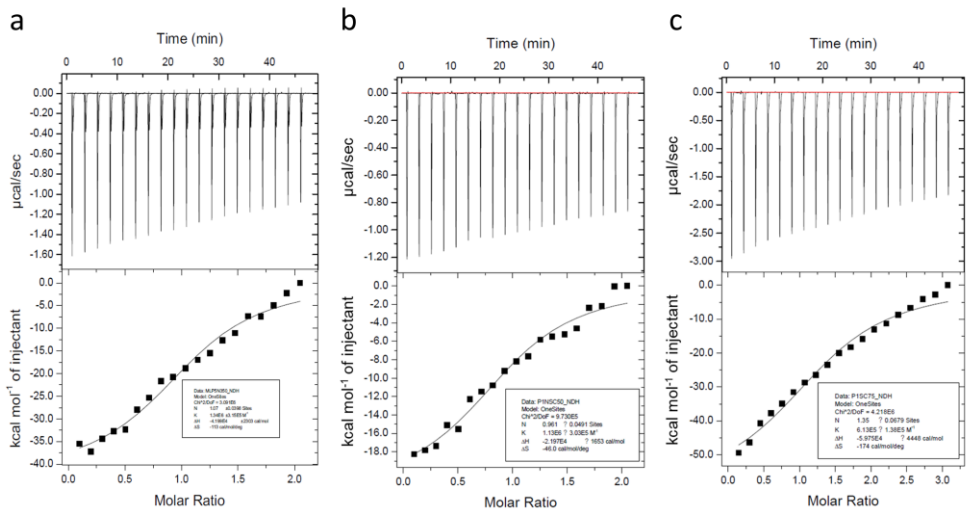

Figure 3-5. ITC measurement of p53TAD and MDM2 interaction inhibitors. The dissociation constant (K_d) was determined by titrating 50 μM of Nutlin-3 (a), 50 μM of NSC66811 (b), and 75 μM of SC204072 (c) to 5 μM of MLP sample, respectively. Data provided by KRIBB (Dr. Seung-Wook Chi's group)

Table 3-1. Summary of equilibrium dissociation constant (K_d) values of ITC and nanopore experiments

	K_d (μM)	
Inhibitor	ITC	Nanopore
Nutlin-3	0.79 ± 0.19	0.59 ± 0.04
NSC66811	0.95 ± 0.17	0.81 ± 0.01
SC204072	1.72 ± 0.39	2.65 ± 0.18

3.4. Summary and conclusions

In this chapter, we have demonstrated nanopore detection of all dumbbell shaped protein of mMLP to reveal the detection limit of double-peak signal arising from the translocation of the dumbbell shaped protein in our measurement system. The characteristic type II signal of mMLP can only be distinguishable by characteristic double-peak signal. The reduction of cutoff frequency of low-pass filter below 500 kHz significantly distorted the peak shape of nanopore signal, thereby the double-peak could not be resolved and detected as a type I signal. We also found that even f_c > 500 kHz, the type I event is still appeared, revealing the limitation of the measurement system. The revealed maximum type II fraction in mMLP translocation event shows f_{mMLP} = 0.84. Also, we proved that the structural change of MLP is caused by the inhibition of p53/MDM2 interaction and the molecular structure of tMLP and mMLP is identical by analyzing intra-peak of type II event in tMLP and mMLP translocation signal. Next, we evaluated binding affinity of the small-molecule inhibitors by detecting type II fraction. Based on the simple binding curve, the K_d value for Nutlin-3, NSC66811, and SC204072 were estimated. Also, the nanopore results were compared with an alternative titration technique of isothermal titration calorimetry, showing that our single-molecule approach for nanopore titration by counting individual, structure-based signal is in agreement to the ITC result. Our nanopore result might contribute to applications for drug screening with ultra-sensitive, high throughput measurement and overcome the limitations

of the current titration technologies.

3.5. References

1. Gonzalez, M. W.; Kann, M. G., Chapter 4: Protein interactions and disease. *Plos Comput Biol* **2012,** *8* (12), e1002819.

2. Wells, J. A.; McClendon, C. L. J. N., Reaching for high-hanging fruit in drug discovery at protein–protein interfaces. **2007,** *450* (7172), 1001.

3. Kwak, D. K.; Chae, H.; Lee, M. K.; Ha, J. H.; Goyal, G.; Kim, M. J.; Kim, K. B.; Chi, S. W., Probing the Small-Molecule Inhibition of an Anticancer Therapeutic Protein-Protein Interaction Using a Solid-State Nanopore. *Angewandte Chemie International Edition* **2016,** *55* (19), 5713-5717.

4. Chae, H.; Kwak, D.-K.; Lee, M.-K.; Chi, S.-W.; Kim, K.-B., Solid-state nanopore analysis on conformation change of p53TAD–MDM2 fusion protein induced by protein–protein interaction. *Nanoscale* **2018,** *10* (36), 17227-17235.

5. Kussie, P. H.; Gorina, S.; Marechal, V.; Elenbaas, B.; Moreau, J.; Levine, A. J.; Pavletich, N. P., Structure of the MDM2 oncoprotein bound to the p53 tumor suppressor transactivation domain. *Science* **1996,** *274* (5289), 948-53.

6. Schon, O.; Friedler, A.; Bycroft, M.; Freund, S. M. V.; Fersht, A. R., Molecular mechanism of the interaction between MDM2 and p53. *Journal of Molecular Biology* **2002,** *323* (3), 491-501.

7. Vassilev, L. T.; Vu, B. T.; Graves, B.; Carvajal, D.; Podlaski, F.; Filipovic, Z.; Kong, N.; Kammlott, U.; Lukacs, C.; Klein, C.;

Fotouhi, N.; Liu, E. A., In vivo activation of the p53 pathway by small-molecule antagonists of MDM2. *Science* **2004,** *303* (5659), 844-8.

8. Chae, H.; Kwak, D.-K.; Lee, M.-K.; Chi, S.-W.; Kim, K.-B. J. N., Solid-state nanopore analysis on conformation change of p53TAD–MDM2 fusion protein induced by protein–protein interaction. **2018,** *10* (36), 17227-17235.

9. Lee, M. H.; Kumar, A.; Park, K. B.; Cho, S. Y.; Kim, H. M.; Lim, M. C.; Kim, Y. R.; Kim, K. B., A low-noise solid-state nanopore platform based on a highly insulating substrate. *Sci Rep* **2014,** *4*, 7448.

10. Plesa, C.; Kowalczyk, S. W.; Zinsmeester, R.; Grosberg, A. Y.; Rabin, Y.; Dekker, C., Fast translocation of proteins through solid state nanopores. *Nano letters* **2013,** *13* (2), 658-663.

Chapter 4. Summary and Conclusions

In the chapter 1, the basics of solid-state nanopore and principle are introduced. The characteristic of protein molecule and its analysis by using solid-state nanopore are discussed. The measurement of biophysical properties such as net charge, conformation, molecular weight, folding/unfolding state, and protein-protein interactions using nanopores are discussed. Although these properties are successfully detected, there have been issues of solid-state nanopore for protein sensing: fast translocation speed of protein and the lack of temporal resolution for the measurement system. It is still currently investigated to reduce speed of protein molecule with improved hardware capability for detecting such a small, fast traversing protein molecule. Next, the drug screening concept and it limitation in terms of measurement technique was discussed. Since solid-state nanopores detect a single molecule translocation, several research works about molecular interaction of protein using solid-state nanopore are discussed.

In the chapter 2, an advanced nanopore detection of protein-protein interaction and its inhibition method is discussed. In the previous chapter, Kwak *et al*. have proved the protein-protein interaction by monitoring change in event frequency upon reversing the net charge of MDM2 molecule, but the change in net charge upon protein-protein interaction is not generally induced because there are plenty of protein-protein interactions without changing its net charge. Thus, in this chapter, the

change in conformation in a single molecule protein was detected by connecting amino acid liker between p53 and MDM2 (MLP). While the globular shaped MLP showed single-peak signal (type I), translocation signal of the linker elongated form by addition of Nutlin-3 (tMLP) was successfully distinguished by a characteristic double-peak signal (type II). The transport kinetics of differently structured MLP and tMLP by introducing 1D diffusion-drift model, revealing that the different diffusivity of the proteins led to the transport kinetics. To discover the diffusivity actually caused the transport kinetics of two proteins, the voltage dependency of translocation rate was investigated. In this experiment, the capture rate of two type of proteins showed the linear dependency to the applied voltage showing that the transport of the proteins in the nanopore system is limited by diffusion process, which is in agreement with the Smoluchowski relation. Finally, owing to the low electrical noise nanopore device, the local peak of the intra-peak of the double peak signal, caused by the dumbbell shaped tMLP translocation, was successfully analyzed.

In the chapter 3, the measurement of binding affinity of three different potential inhibitors to the p53 and MDM2 interaction are demonstrated. In order to figure out the accuracy of nanopore detection for the double-peak signal arise from the dumbbell shaped tMLP, mutant MLP (mMLP) was introduced by replacing p53TAD into $(GGGS)_3GGS$, in that there is no binding motif to the MDM2, thereby exhibit dumbbell shape without any

inhibitor treatment. In the mMLP experiment, the maximum type II fraction was measured as ~0.84 at 500 kHz of cut-off frequency. Next, the binding affinity was measured by monitoring increase in type II fraction by increasing the concentration of inhibitors (Nutlin-3, NSC66811, and SC204072). Upon increasing the inhibitor concentration, the increased type II fraction was measured and fitted by the binding equation, yielding the equilibrium dissociation constant of 594 ± 39, 807 ± 12, and 2650 ± 177 nM for Nutlin-3, NSC66811, and SC204072, respectively. No such increase was observed in the negative control of MMC chemical, which is known not to bind into MDM2. Finally, the binding affinity of the inhibitors was measured by isothermal titration calorimetry (ITC) and compared with the nanopore results. These two results show consistent K_d values, implying that the nanopore detection exhibit an equivalent tool for measuring binding affinity of small molecule inhibitor of protein-protein interactions with the existing technique and thus, suggesting that nanopore technique can be a valuable method in discovering inhibitor molecule in protein-protein interfaces.

Abstract (in Korean)

초고속 및 고효율 전기적 판독 특성을 갖는 나노포어 기술은 단일 분자 수준의 분해능으로 생체 분자의 생물-물리학적 특성을 분석하는 기술로 발전하고 있다. 지난 10 년 동안 solid-state nanopore에 대한 연구는 DNA의 transport phenomena에 집중되어 왔는데, 그 중에서도 특히 DNA의 염기서열 분석에 초점을 맞추었다. 서로 다른 핵산 간의 물리적 크기 차이를 나노포어 신호의 차이로 구별하고자 하였으나, 나노포어의 공간, 시간 분해능의 부족 및 전기적 노이즈의 발생으로 인해 어려움을 겪고 있다.

최근에는 DNA가 아닌 단백질에 대한 나노포어 분석이 대두되고 있다. 단백질은 DNA와는 다르게 3차원 구조를 가지고 있고, DNA의 핵산보다 상대적으로 물리적 크기가 크기 때문에 비교적 낮은 공간, 시간분해능과 노이즈를 포함한 소자에서도 분석이 가능하다. 단백질은 다른 분자와의 결합을 통해 생체기능을 수행하는 생체분자로서, 단분자 단백질 신호를 측정하는 것은 생명현상의 기초원리를 밝혀줄 중요한 단서를 제공해준다.

나노포어는 단분자 생체물질의 통과신호로부터 전기적 판독 특성을 가지기 때문에, 최근에는 단백질의 분석에 solid-state nanopore가 활용되고있다. 본 dissertation에서는 i) 단백질 - 단백질 상호 작용 (PPIs)과 저분자 약물에 의한 억제, ii) PPI의 억제에 의해 유도 된 구조 변화, iii) 단백질 구조변화 기반 나노포어 적정을 통한 결합평형상수 측정에 대한 내용을 다루었다.

첫번째로, solid-state nanopore를 사용하여 항암 표적 단백질인 p53 transactivation 도메인 (p53TAD)와 mouse double minute 2 (MDM2) 사이의 상호 작용을 모니터링했습니다. 또한 이 상호작용의 Nutlin-3에 의한 억제를 나노

포어 신호의 빈도로서 측정했다. MDM2 (isoelectric point; pI = 9.0)는 수용액 속에서 양전하를 띄고있고 전극에 음전압에 발생한 전기장에 의해 전기영동력에 의해 나노포어를 통과하게 된다. 그러나 음전하를 띈 p53TAD (pI = 3.6)와의 상호 작용의 결과로 MDM2의 전하가 음으로 변경되어 MDM2의 나노포어 통과신호의 빈도가 크게 감소한 것을 확인했다. 이 단계에서, p53TAD / MDM2 복합체에 Nutlin-3를 첨가하면 p53TAD / MDM2의 상호 작용이 억제되어 MDM2가 복합체에서 분리된다. 이 경우, MDM2와 복합체에서 분리되어 나온 MDM2 모두의 통과신호가 발생하기 때문에 나노포어 통과신호의 회복을 관찰할 수 있었다. 그러나, 이 접근법은 MDM2의 전하의 변화가 반드시 수반되어야 하는 시스템이기 때문에 단백질 시스템의 선정에 한계가 있다.

두번째로, 기존 나노포어 신호 빈도를 모니터링 하는 기존 방법을 보완하고자, 고체 상태 나노 기공을 사용하여 p53TAD-MDM2 융합 단백질의 약물에 의해 유도 되는 구조 변화를 모니터링하려고 시도했다. 단백질-단백질 상호 작용으로 인한 구조 변화를 효과적으로 감지하기 위해 p53TAD와 MDM2가 16 개 아미노산 linker로 연결된 융합 단백질 MLP (MDM2- linker -p53TAD)를 디자인 했다. MLP의 구형 형태는 single-peak (type I)을 보였으나 Nutlin-3에 의해 p53TAD와 MDM2 사이의 상호작용이 억제되어 linker가 풀어짐으로 인해 MLP는 덤벨 형태를 가지게 되고, 이에 의한 나노포어 통과신호는 double-peak signal (type II)로 나타났다. Nutlin-3 농도가 증가함에 따라 double-peak 대 single-peak 신호의 비율은 9.3 %에서 23.0 %로 증가는 것을 보였다. 또한 전압에 따라 type I과 type II 신호를 분석하여 서로 다른 구조를 가지는 단백질이 나노포어를 통과할 때 나타나는 동역학적 현상을 (translocation kinetics)이 분석했다. 또한 double-peak 신호 내부의 intra-peak의 크기를 분석하여 디자인한 단백질 복합체의 구

조를 분석할 수 있었다.

마지막 part에서는, 약물 분자의 binding affinity를 정량적으로 평가하기 위해 세 가지 다른 small-molecule 약물 (Nutlin-3, NSC66811 및 SC204072)의 MLP에 대한 열역학적 평형상수를 측정했다. 측정 시스템에서 double-peak 신호를 구별하기 위해, 본 측정 시스템이 가지는 분해능의 한계를 분석해야한다. 이를 위해 p53TAD (residue 15-29)를 $(GGGS)_3GGS$ 로 대체하여, MLP 가 약물 없이도 dumbbell 형태를 지니는 복합체 (mutant MLP; mMLP)를 디자인했다. mMLP에서는 type I signal 대비 type II 신호의 최대 비율이 ~ 0.84로 나타났으며, 이는 본 측정 시스템에 대한 해상도의 한계를 의미하고 있다. 약물 분자에 의해 유도 된 MLP의 구조 변화로부터 type II fraction의 증가에 기반하여, 각 약물 분자에 의한 MLP 단백질에서 나타나는 type II fraction을 관찰 하였다. Type II fraction data에 결합 모델을 fitting하여 Nutlin-3, NSC66811 및 SC204072 각각에 대해 594 ± 39, 807 ± 12 및 2650 ± 177 nM의 K_d 값을 성공적으로 얻을 수 있었다. 위 결과는 isothermal titration calorimetry 실험 결과와 비교했을 때 유사한 값을 보여 주었으며, 나노포어가 가지는 단분자 측정, 극소량의 시료로도 측정이 가능하다는 점을 감안하면 기존 drug screening 기술의 한계점을 보완할 수 있는 장점을 가진 기술이라고 할 수 있다.

List of publications

Papers

1. Dong-Kyu Kwak, **Hongsik Chae**, Mi-Kyung Lee, Ji-Hyang Ha, Gaurav Goyal, Min Jun Kim, Ki-Bum Kim, and Seung-Wook Chi, "Probing the Small-Molecule Inhibition of an Anticancer Therapeutic Protein-Protein Interaction Using a Solid-State Nanopore", Angewandte Chemie International Edition 2016, 55 (19), 5713-5717.
2. Kyeong-Beom Park, Hyung-Jun Kim, Yun-Ho Kang, Jae-Seok Yu, **Hongsik Chae**, Kidan Lee, Hyun-Mi Kim, and Ki-Bum Kim, "Highly reliable and low-noise solid-state nanopores with an atomic layer deposited ZnO membrane on a quartz substrate", Nanoscale 2017, 9 (47), 18772-18780.
3. **Hongsik Chae**, Dong-Kyu Kwak, Mi-Kyung Lee, Seung-Wook Chi, Ki-Bum Kim, "Solid-state nanopore analysis on conformation change of p53TAD–MDM2 fusion protein induced by protein–protein interaction", Nanoscale 2018, 10 (36), 17227-17235.
4. Kidan Lee, Kyeong-Beom Park, Hyung-Jun Kim, Jae-Seok Yu, **Hongsik Chae**, Hyun-Mi Kim, and Ki-Bum Kim, "Recent Progress in Solid-State Nanopores", Advanced Materials 2018, 30 (42), 1704680.
5. **Hongsik Chae**, Dong-Kyu Kwak, Mi-Kyung Lee, Seung-Wook Chi,

Ki-Bum Kim, “Nanopore Analysis on the Drug-Induced Conformation Change of a p53-Linker-MDM2 Protein Complex”, Journal of Nanoscience and Nanotechnology. *Just accepted*

Patents

1. 미국 CIP

“METHODS FOR ANALYZING PROTEIN-PROTEIN INTERACTIONS AND SCREENING PROTEIN-PROTEIN INTERACTION INHIBITORS USING NANOPORES”

발명자: 지승욱, 김기범, 곽동규, 채홍식, 이미경, 하지향 (출원번호: 16/043,980)

2. PCT

“나노포어를 이용한 단백질-단백질 상호작용 저해제 스크리닝 방법”

발명자: 지승욱, 김기범, 곽동규, 채홍식, 이미경, 하지향 (출원번호: PCT/KR2016/001113)

2. 대한민국

“나노포어를 이용한 단백질-단백질 상호작용 저해제 스크리닝 방법”

발명자: 지승욱, 김기범, 곽동규, 채홍식, 이미경, 하지향 (등록번호: 10-2016-0009577)

Conferences

1. **Hongsik Chae**, Dong-Kyu Kwak, Hyun-Mi Kim, Kyeong-Beom Park, Jung-Mo Yeo, Hyung-Jun Kim, Jae-Seok Yu, Kidan Lee, Ki-Bum Kim, and Seung-Wook Chi, "Protein translocation analysis by using solid-state nanopore", **ENGE 2014**
2. **Hongsik Chae**, Dong-Kyu Kwak, Mi-Kyung Lee, Ji-Hyang Ha, Gaurav Goyal, Min Jun Kim, Ki-Bum Kim, and Seung-Wook Chi, "Nanopore analysis on small-molecule inhibition of anticancer protein-protein interaction", **Nano Convergence 2016 (AWARDED)**
3. **Hongsik Chae**, Dong-Kyu Kwak, Mi-Kyung Lee, Ji-Hyang Ha, Gaurav Goyal, Min Jun Kim, Ki-Bum Kim, and Seung-Wook Chi, "Probing the Small-Molecule Inhibition of an Anticancer Therapeutic Protein-Protein Interaction Using a Solid-State Nanopore", **ECS PRiME 2016**
4. **Hongsik Chae**, Dong-Kyu Kwak, Mi-Kyung Lee, Ji-Hyang Ha, Gaurav Goyal, Min Jun Kim, Ki-Bum Kim, and Seung-Wook Chi, "Probing the Small-Molecule Inhibition of an Anticancer Therapeutic Protein-Protein Interaction Using a Solid-State Nanopore", **NANO KOREA 2016**
5. **Hongsik Chae**, Dong-Kyu Kwak, Mi-Kyung Lee, Ji-Hyang Ha,

Gaurav Goyal, Min Jun Kim, Ki-Bum Kim, and Seung-Wook Chi, "Protein Detection by Using Solid-State Nanopore: Inhibition of an Anticancer Therapeutic Protein-Protein Interaction" **Nano Convergence 2017**

6. **Hongsik Chae**, Dong-Kyu Kwak, Mi-Kyung Lee, Ji-Hyang Ha, Gaurav Goyal, Min Jun Kim, Ki-Bum Kim, and Seung-Wook Chi, "Protein Detection by Using Solid-State Nanopore: Inhibition of an Anticancer Therapeutic Protein-Protein Interaction", **WE-Heraeus-Seminar 2017 (Transport Mechanisms in Biological and Synthetic Nanopores and channels)**
7. **Hongsik Chae**, Dong-Kyu Kwak, Mi-Kyung Lee, Seung-Wook Chi, and Ki-Bum Kim, "Nanopore Analysis on Protein-Protein Interaction: Drug-induced conformational change of proteins", **ENGE 2018**